HHS Public Access

Author manuscript

IEEE Microw Mag. Author manuscript; available in PMC 2021 June 23.

Published in final edited form as:

IEEE Microw Mag. 2020 May ; 21(5): 94–119. doi:10.1109/mmm.2020.2971375.

Advances in Microwave Near-Field Imaging: Prototypes, Systems, and Applications

Wenyi Shao,

Johns Hopkins University, Baltimore, Maryland, United States.

Todd McCollough

Ellumen, Inc., Arlington, Virginia, United States.

Abstract

Microwave imaging employs detection techniques to evaluate hidden or embedded objects in a structure or media using electro-magnetic (EM) waves in the microwave range, 300 MHz–300 GHz. Microwave imaging is often associated with radar detection such as target location and tracking, weather-pattern recognition, and underground surveillance, which are far-field applications. In recent years, due to microwaves' ability to penetrate optically opaque media, short-range applications, including medical imaging, nondestructive testing (NDT) and quality evaluation, through-the-wall imaging, and security screening, have been developed. Microwave near-field imaging most often occurs when detecting the profile of an object within the short range (when the distance from the sensor to the object is less than one wavelength to several wavelengths) and depends on the electrical size of the antenna(s) and target.

A near-field microwave-imaging system attempts to reveal the presence of an object and/or an electrical-property distribution by measuring the scattered field from many positions. Typically, numerous sensors are placed near the object, and a quantitative or qualitative algorithm is applied to the collected data. Due to hardware-technology limitations, such as the unavailability of a data-acquisition apparatus, along with limited computational resources, early work in experimental microwave imaging was challenging. Examples include the canine kidney imaging experiment conducted by Jacobi and Larsen during the 1970s [1]–[3] and the active microwave imaging of a horse kidney by Jofre and Bolomey [4]. During the 1990s, researchers were able to use microwave signals higher than 1 GHz in experimental imaging systems. Bolomey and Pichot developed a practical system for active microwave imaging [5] and designed a planar microwave camera, both operating at 2.45 GHz [6]. However, probably due to the hardware cost, most studies (operating at a few gigahertz) were still focused on software only.

During the past few decades, the hardware and software components of a near-field microwave-imaging-system technology have attracted interest throughout the world. The feasibility of using microwave approaches to image different types of objects has been tested and verified by simulations in a variety of applications. Further, work has been conducted on

wshao8@jhu.edu.

bettering quantitative and qualitative algorithms to improve simulated reconstruction results. Benefitting from hardware improvements and cost reductions, researchers are eager to pursue real-world experimental validation instead of simulations, and more unique prototypes and commercial systems have been built for various applications. These prototypes and systems are the result of years of dedicated work, and it is important to consider the advancements in developed prototype systems. This article reviews many of the systems designed by different research groups around the world for near-field microwave-imaging applications. It outlines current challenges in microwave near-field imaging, areas of developmental interest, and microwave near-field imaging's outlook for the future.

Microwave Medical Imaging

Microwave imaging for medical applications has attracted significant interest during the past 20 years. The physics behind microwave medical imaging relates to the fact that the dielectric properties of abnormal tissue (for example, malignant tissue) are significantly different than those of normal tissue at microwave frequencies. This difference results in a noticeable contrast in the reconstructed microwave image. Current studies typically focus on the range of 500 MHz–10 GHz to balance the tradeoff between penetration depth and image resolution.

According to the various acquisition setups, the measurement system can be in a passive or active mode. Passive-mode systems exploit the principles of radiometry [1]–[10] to produce an image of the natural microwave radiation from human tissue. In active-mode systems, microwave radiation is directed toward tissue, and the scattered EM fields are detected and processed. As early as 2000, at Dartmouth College, Meaney's group [11] reported the first clinical prototype for active near-field microwave imaging of the breast. The researchers implemented 16 monopoles in a ring to transmit and receive microwave signals in the 300–1,000-MHz range. Tomographic images were created for seven heights as the ring was moved from the chest wall toward the nipple. This system set the stage for later developments in active-mode microwave medical imaging. The group's research has been reviewed in several papers and textbooks [7]–[23] and three times in this magazine [12]–[14], providing many details of microwave imaging technology.

Since the purpose of this article is to review hardware microwave-imaging systems, the discussion in this section briefly addresses some older systems included in prior reviews to provide historical perspective. The particular focus is on recent active-mode hardware systems for two prominent medical applications currently under investigation: early stage breast-cancer and brain-injury detection.

Microwave Breast Imaging

Cost reductions in RF manufacturing have enabled many microwave breast-imaging systems to operate at a few gigahertz to obtain a high resolution where the dielectric property provides a significant contrast between malignant and healthy states for some breast tissues, with the notable exception of fibroglandular tissue [24]. In 2007, Meaney's group reported an optimized imaging system [shown in Figure 1(a)] [25]. The patient was examined in a downward-facing position with the breast suspended (through a hole in the examination

table) in a tank of coupling liquid composed of glycerin and water, providing a better impedance match than the water-only coupling liquid used in the group's earlier system [11]. A multistatic-mode system was used, with one antenna in the array serving as a transmitter, while the others were receivers. Meaney's group also reported an application to detect a target inclusion immersed in a plastic breast phantom filled with glycerin and water [26]. The plastic breast-shaped phantom, pictured in Figure 1(b) and (c), was made according to magnetic resonance scans of a real breast. The permittivity of the target inclusion and background medium (the glycerin and water mixture) at 1,500 MHz was 48.88 and 19.8, respectively [27].

The third generation (3G) of the Meaney group's system, reported in 2014, used a local-oscillator (LO) network and an analog-to-digital (AD) board, as illustrated in Figure 1(d) and (g), where the illumination tank, antenna array, and motion-control hardware are reconfigured into a low-profile ergonomic module that enables the independent movement of the antennaarray subsets to arbitrary heights for the acquisition of in-plane and cross-plane (XP) transmissions. A 3D reconstruction was made for the permittivity and conductivity of the breast phantom, as shown in Figure 1(e) and (f), at varying XP distances. The target inclusion can be clearly seen in the image reconstructed with a microwave tomography approach where dielectric values were found. Since 2014, many follow-up in vivo studies of the Meaney technique have been conducted, with one exploring chemotherapy [28].

At the University of Wisconsin, Hagness and her colleagues developed a microwave breast-imaging system for use with experimental breast phantoms using their microwave-imaging-via-space–time beamforming approach. A sole ultrawideband (UWB) antenna served as the transmitter and receiver. An image of the experimental breast phantom accurately located two 4-mm-diameter synthetic tumors separated by approximately 2 cm [29].

A more advanced microwave breast-imaging system was developed at the University of Bristol by Craddock and his colleagues [30]–[33], as shown in Figure 2(a) and (b). The breast was placed in a hemispherical cup, and a good match to the antennas was provided using a layer of fluid, which could be replaced by a ceramic insert. The first design used 31 UWB slot antennas in the array [30]–[32], and a later design increased the number of antenna elements to 60 [33]. The antenna array was connected to a switching network before it was joined to an eight-port vector network analyzer (VNA), facilitating a rapid scan of up to 8 GHz. The later system could acquire 1,770 unique S-parameter measurements in a mere 10 s. In contrast, the earlier system, with a two-port VNA, could acquire only 65 S-parameter measurements in 90 s. Thus, the later system reduced the chance that noise would result from any slight patient movement. In 2011, the system was used for a clinical evaluation of 95 patients [34], followed by another with 86 patients in 2016 that achieved a detection rate of 74% (64/86) for a wide age range and 86% detection in dense breasts [35]. The result was encouraging since it was comparable to or better than outcomes reported from digital-mammographic-imaging screening trials. The Craddock group's work opens the possibility of large-scale clinical trials.

At the University of Calgary, Fear and her colleagues developed a prototype system for radar-based breast imaging, with a patient table similar to the one developed at Dartmouth.

A woman lies with one of her breasts suspended through a hole in an examination table. A tank containing immersion liquid, a UWB transceiver antenna [36], and a laser is located under the examination table [37]. The UWB antenna and laser are mounted on an arm that can rotate around the center of the tank and move in the vertical direction, as pictured in Figure 3(c) and (d), to achieve an effect equivalent to using an antenna array. The laser scans the 3D surface of the breast and defines the reconstruction volume. The UWB antenna, operating in a monostatic mode, sends and receives microwave signals across the frequency range 2.4–15 GHz, but the VNA records data in the 50 MHz–15 GHz range before they are converted to the time domain for processing [38]. Fear and her group created 3D images for eight subjects using a confocal-imaging algorithm [39] developed by Hagness et al.

In the second generation (2G) of their system, Fear and her colleagues used a laser to precisely place the antenna in an adaptive matter so that the microwaves were normally incident on the skin [40]. Such a design may deliver more microwave energy to the breast and thus significantly increase the signal-to-noise ratio. Fear and her group developed another system for breast-tissue dielectric-permittivity estimation [41]. Instead of using coupling liquid, direct contact is made between the breast skin and sensor array. It will be interesting to see the competition between the different mechanisms developed by the same group.

Using a VNA (especially one with multiple ports) with a microwave-imaging system greatly increases the system cost and size. Persson’s research group at the Chalmers University of Technology (CUT) developed a compact imaging system for medical diagnostics that does not use a VNA [42]–[44]. Instead, the time-domain system contains an impulse generator (to transmit UWB pulses), a high-speed AD converter (ADC) to sample the analog data collected by the antenna, and a field-programmable gate array (FPGA) to store and process digital data and control the entire measurement. To solve the problem of the ADC’s insufficient bandwidth (800 MHz), a WB track-and-hold (T/H) circuit monitors and freezes the received signal ahead of the ADC and maintains it for the ADC to sample. In addition, a direct digital synthesizer (DDS) generates sampling instructions for the T/H and ADC.

The signal receiver and antenna array developed at CUT are illustrated in Figure 4. The antenna array was composed of 20 monopoles evenly distributed in a circle, and no coupling medium was used. A switching matrix was employed to select transmitting- and receiving-antenna pairs in the array. Finally, a 2D time-domain inverse algorithm was implemented to reconstruct a dielectric image, as pictured in Figure 4(c), when a cup of vegetable oil was placed in the middle of the circle. Although no clinical test was performed and it is unclear which disease the developed system targeted, replacing the VNA with a customized receiver system was an advance.

A similar data-acquisition unit was reported by Rubaek et al. [45], from the same department at CUT and in conjunction with the Technical University of Denmark, for breast-cancer detection, as shown in Figure 4(d). The system uses an antenna array consisting of 32 monopoles horizontally positioned in a tank filled with glycerin and water. The monopoles are arranged in four rows of eight. Instead of using an FPGA, the data are stored in a computer where the signal processing is accomplished with LabView software. Furthermore,

an RF signal generator is used with an ADC. Since a synthetic aperture radar (SAR) aperture is also created in the vertical direction, the system is able to render a 3D image of the object under test, in contrast to the 2D view that Persson's group reconstructed. Rubaek et al.'s targeted images included water-filled plastic spheres.

Time-domain measurements may offer advantages over frequency-domain measurements, including faster scan times and more cost-effective measurement devices. Popovic and her team at McGill University developed time-domain microwave-imaging systems for breasts [47]–[52]. In the first [47]–[51], 16 antennas were inserted in slots along the outer surface of a hemispherical radome, as pictured in Figure 5(a) and (b), enabling the transmission and recording of co- and cross-polarized pulses using a bandwidth from 2 to 4 GHz. The radome was an aluminum bowl in which a breast was placed. To fit women with various breast sizes, the radome was designed to accommodate the largest anticipated size, and an immersion medium was used for smaller breasts to avoid air gaps. However, the lossy immersion medium attenuated the responses and added additional reflection interfaces between the antenna and breast.

In a later design, a wearable antenna array consisting of 16 monopoles was embedded in a bra, as shown in Figure 5(c) [52], that went through two stages of refinement [53]. The antennas were on the inside of the bra and tangential to the skin surface. Thus, they touched the skin directly, and there was no need for an immersion medium. The scan process was a typical multistatic mode in the time domain: a pulse was generated and fed to a switching network that selected the transmitting and receiving antennas; the received signal was recorded by a picoscope. A complete scan consisting of 16 × 15 signals took roughly 6 min. The bra-based system was tested on a healthy volunteer over the course of 28 days for breast-health monitoring [52]. Consistent imaging results demonstrated that the data collected by the bra-based system had good repeatability. A clinical trial including 13 patients was performed [50], [51].

Another notable example of microwave imaging for breasts was reported by Vipianna and colleagues at Politecnico di Torino [54]–[56]. Like the CUT group, the system Vipianna et al. developed used an embedded platform enhanced with an FPGA to receive and process signals, making the system more practical and commercially viable. Additionally, the signal-processing speed of the FPGA was 20 times faster than on a multicore CPU, enabling more rapid image reconstructions. Figure 6(a) illustrates the architecture of the prototype system. Breast phantoms were scanned in a coupling liquid (a glycerin and water mixture) in which the antennas were specifically designed to work. Only a 200-MHz bandwidth between 1.4 and 1.6 GHz was needed to produce a fairly good image, due to the use of an interferometric multiple-signal-classification (MUSIC) algorithm, which does not require a large bandwidth to detect scattering inside the breast. The system could be cost-effectively produced since electronic components in the frequency range of interest are available for low prices.

In Japan, Kikkawa's group reported a hand-held impulse radar detector for breast-tumor location [57]. The probe is a 4 × 4 cross-shaped dome antenna array operating in the UWB frequency range, 3.1–10.6 GHz, which facilitates the transmission of Gaussian monocycle pulses with a width of 160 ps. The detector is designed to be placed on the breast with the

patient in a supine position. Figure 7(a) shows the bowl-type probe, and Figure 7(b) displays the architecture of the detector. A step motor mounted on the top of the detector drives the system, including rotating the dome antenna array with one-degree accuracy. A plastic cover is installed on the antenna dome to protect the patient and mitigate friction during rotation, as depicted in Figure 7(b) and (c). The acquired analog signal is sampled by an ADC with 12-b accuracy for a high resolution. The pulse generator, switching matrix, and sampling module are integrated on the CMOS circuit with 65-nm technology. Because of these modules, the impulse radar imaging system is much more compact than the previously discussed devices. The detector is connected to a computer by a USB cable for data collection and processing. The confocal algorithm is used for processing the saved data to generate an image.

It is worth mentioning three additional systems inspired by Meaney's group, where the patient lies on an examination table with the breast placed through an opening. The first was developed by Jeon's group at the Electronics and Telecommunications Research Institute in Korea [58]. This system was evaluated on five dogs, three of which had breast tumors [60]. Another was developed by Chen's group at the Southern University of Science and Technology, China, with results presented from the first phase of a clinical trial that included 11 Asian women [61]. The third was devised by Kuwahara's group at Shizuoka University, Japan, including three antenna arrangements to accommodate different breast sizes [62], [63].

Table 1 compares the microwave breast-imaging systems described previously. It highlights differences between the number and type of antennas used, frequencies of operation, hardware, and use of a coupling liquid. Many of the systems rely on a VNA, but some have moved toward using an ADC. Two systems operate in a monostatic mode, which avoids the mutual coupling of adjacent antenna elements. Until recently, commercial network analyzers had a limited dynamic range for imaging dense breast tissue [27]. Oscillo-scopes also suffer from a limited dynamic range for imaging small tumors in the breast [121].

Microwave Brain Imaging

A microwave method for human-brain imaging has not attracted quite as much interest as microwave breast imaging. Current microwave brain-imaging technology is based upon studies showing that tissue malignancies, the blood supply, hypoxia, acute ischemia, and chronic infarction significantly change the dielectric properties of the affected cerebral tissue at microwave frequencies [64]. By exposing brain tissue to a low level of microwave energy and capturing the scattered signal with an antenna, estimates of the tissue's dielectric profiles can be made.

Pioneering research in microwave brain imaging can be traced to Lin and Clark's 1982 work [65], in which the detection of cerebral edema (an accumulation of water in the brain) was experimentally tested using a 2.4-GHz microwave signal through a simple head phantom. Modern active-mode microwave imaging for a brain or head scan was first published in 2008, with Semenov's study at Keele University [66] and Persson's research at CUT [67]. Semenov simulated microwave measurements with 32 × 32 or 64 × 64 transmitters and receivers (multistatic mode) for a 2D model of a head with a radius of 11 cm and that

contained a few soft tissues, skull, and small stroke area. The data were processed through an image-reconstruction procedure using the Newton approach [68] across a frequency range of 0.5–2.5 GHz. A stroke-like area with a radius of 2 cm was seen in the image reconstructed at a 1-GHz frequency. Semenov warned against the use of wavelengths above 1 GHz for microwave brain tomography because of high micro-wave-energy attenuation in the brain.

In early work by Persson's group, a low-cost patch antenna with a triangular shape was designed to be small and lightweight and potentially serve as the antenna element in an array for brain-stroke monitoring. To improve the impedance matching, a liquid with a relative permittivity of 78 was used, placed in a bag between the antenna and head (for the high-frequency case) or with the antenna immersed in the fluid (for the low-frequency case). A system containing eight such antennas spaced at varying distances was designed and simulated for an overall performance characterization. A later development involved a fabricated array on a helmet placed on the head [69]. The array elements ranged from 10 in the first generation to 12 in the 2G and 8 in the 3G, as illustrated in Figure 8(a), (b), and (c), respectively.

Four intracranial-bleeding head phantoms (modeled to have varying levels of subdural hematomas: 0, 40, 70, and 110 mL) were created using solutions of water, sugar, agar, and salt that mimicked the dielectric properties of blood and gray brain matter [70]. Thirty measurements were performed with the 2G system on each phantom, for a total of 120 (with two of the 12 antennas unused), in the frequency range 0.1–3 GHz. A classification algorithm based on singular-value decomposition was implemented, and 100% accuracy was achieved, since all the observations had the shortest subspace distance to their respective bleeding-class level. Using the 3G system, a clinical evaluation was performed on 20 patients with chronic subdural hematomas. The study showed a high classification accuracy, with a receiver operating characteristic (ROC) curve that had an area under the curve (AUC) of 0.94 [71].

At the University of Queensland, Australia, brain imaging for stroke-injuries detection has been intensively studied by Abbosh and his group [72]–[76]. They developed their first detection system [72], [74] in 2013; it appears in Figure 9(b). Sixteen corrugated tapered-slot antennas (operating at a frequency from 1 to 4 GHz) are fixed on a table and equally distributed around a head phantom, with a fixed distance of 5 mm from the head boundary. The antennas work in a monostatic mode. To increase the number of signals to be processed during image reconstruction without adding antennas (to avoid unwanted mutual coupling), the table can rotate to collect data from different angle positions.

To carry out a practical brain-scan measurement, a realistic 3D head phantom was built, as shown in Figure 9(a), consisting of a suitable mixture of water, corn flour, gelatin, agar, sodium azide, and propylene glycol to mimic different brain tissues with realistic dielectric properties. The dielectric properties of the fabricated tissues agreed with measurements that had a less than 3% error across the frequency band from 1 to 4 GHz. An ellipsoid object with dielectric properties equivalent to blood was emulated as the stroke region and inserted inside the head phantom. S-parameters were collected using a VNA, and algorithms were

implemented to reconstruct 2D images. High-contrast stroke regions were successfully localized. Due to steep energy losses in the head at high frequencies, the antenna elements in later work were replaced by compact unidirectional antennas with an operating frequency between 1.1 and 2.2 GHz [76], which provides a compromise between the penetration depth and image resolution.

The second system developed by Abbosh's group uses only one unidirectional antenna covering a frequency band from 1.1 to 3.4 GHz to send and receive signals to and from the head phantom, which is placed on a rotatable support, as pictured in Figure 9(c). A portable, custom-made microwave transceiver, Agilent N7081A, replaces a VNA to send and receive signals. The N7081A is a small, high-speed, low-cost modular WB transceiver device that can operate across a bandwidth from 0.1 MHz to 4 GHz and offers a maximum dynamic range of 80 dB. It is controlled by an in-home operation system installed on a PC via USB or local-area network connections for postprocessing data. In the third system developed by Abbosh's group, a fixed array is used, with 16 antennas operating in a frequency band of 1 to 2.4 GHz. Two healthy volunteers' heads were scanned at three levels, and the reconstructed images displayed no hematomas [77].

A brain-stroke imaging prototype system has been developed by EMTensor, a company founded by Semenov that has collaborated with Pichot and his colleagues at the Université Côte d'Azur, France [78], [79]. The system consists of a cylindrical metallic chamber composed of five rings of 32 transmitting and receiving antennas, as displayed in Figure 10(a). The antennas are ceramicloaded, open-ended waveguides operating from 0.9 to 1.8 GHz. The system operates in a multistatic mode, using a switching matrix to connect the antennas and a network analyzer, which results in a 160 × 160 matrix of S-parameters. The data-acquisition cycle of the system is electronically controlled, enabling the process to complete in roughly 30 s. As illustrated in Figure 10(b) and (c), the chamber is in a horizontal position, which facilitates the easy positioning of a human head within the imaging zone. A special thin membrane isolates the head from a matching liquid, which it contains within the chamber. Two measurements, one with an empty chamber and another with a head, are conducted to obtain the scattered field of the head by subtraction. The collected data are wirelessly transferred to a remote computing center for high-performance postprocessing. Images for a numerical head model have been reconstructed for verification of the developed prototype. Experimental implementation and verification have not been reported.

Table 2 compares the microwave brain-imaging systems described here, highlighting the differences between the number and type of antennas, operation frequencies, hardware, and inclusion of a coupling liquid. As expected, the maximum frequency of operation is typically lower than that of the breast-imaging systems. The reason is that brain tissue is more lossy to microwaves than breast tissue, and, as a result, a lower frequency is used to enable more energy to enter the brain (but this penetration comes at the expense of the imaging resolution).

Other Medical Diagnostic Applications

Besides breast-cancer and brain-stroke imaging, the near-field microwave approach has been applied in medical situations such as extremity injury, bone imaging, and skin- and lung-cancer detection. The knee is one of the most frequently injured joints in the human body, with traumatic injuries in the young and tissue degeneration in the old. Fear et al. utilized a simulation method and some simple experiments to test the feasibility of harnessing radar-based methods at microwave frequencies to detect tears in the meniscus [80], [81], tendon [81], [82], and ligaments [82] of the knee. However, no prototype systems have been reported by her group for diagnosing knee pathologies. Semenov et al. developed a system for extremity soft-tissue imaging [83] and performed measurements on the foreleg of an anesthetized pig [84]. LoVetri's group also developed a system for extremity imaging and reconstructed images of human forearms and bovine legs [85].

Osteoporosis is a major problem affecting those older than 50 that can result in fractured bones. Meaney et al. performed heel exams by adapting their microwave breast-imaging system for aligning the heel in a liquid coupling bath [86], [87]. Two patients were imaged, with encouraging results that showed important anatomical features within the heel and were representative of reasonable microwave-property values [87].

For skin-cancer detection, some early studies utilized microwave reflectometry to differentiate cancerous tissues from healthy ones using an open-ended coaxial probe with a VNA [88], [89]. The reflection co-efficient was compared between cancerous skin tissues and adjacent normal skin tissues from 300 MHz to 6 GHz. Recent studies are more interested in exploring the properties of cancerous skin tissue at the millimeter-wave (mm-wave) range because of the better resolution and absence of deep-penetration requirements for skin measurement. In 2013, Taeb et al. proposed a reflectometry device operating at 42 and 70 GHz for noninvasive, early-stage skin-cancer detection [90]. The device provides a low-cost solution for fast, accurate skin-cancer detection and has the potential to be used for rapid tissue inspection during surgery.

Most of the open-ended rectangular waveguide probes implemented for skin detection have footprints in the range of several square millimeters, and their EM field penetrates deep into the subcutaneous fat; that is, they measure the average of a larger volume compared to the size of early-stage (very small) skin tumors. In fact, malignant melanoma grows from the bottom of the epidermis, typically starting at a depth of roughly 10μm. Therefore, to achieve an accurate measurement, a high-quality mm-wave probe with a submillimeter sensing depth and high lateral resolution is desired. In 2015, Topfer et al. invented a broadband probe operating from 90 to 104 GHz [91] consisting of a dielectricrod waveguide that was metallized and tapered toward the tip to achieve a high resolution by concentrating the electric field in a small sample area. The sensing depth was from 0.3 to 0.4 mm, which was adapted for detecting early stage skin tumors before metastasis. The lateral resolution could be as high as 0.2 mm, enabling the resolution of small skin tumors and even the inhomogeneities within a tumor. In addition to skin-cancer detection, in 2017, Gao et al. used an mm-wave reflectometry approach to accurately assess the degree of a burn on human skin [92]. In the test, mm-wave reflectometry and imaging were verified as capable

of distinguishing between healthy and burned skin, since the dielectric properties of the two are significantly different, in a 26.5–40 GHz frequency band.

Microwave imaging has been explored for lung-cancer detection, based on the hypothesis that a significant difference exists between the dielectric properties of cancerous lung tissue and healthy lung tissue in the microwave frequency band. In Australia, Abbosh's group applied a system similar to the one developed for brain-stroke detection [Figure 9(b)] to perform lung-cancer microwave-imaging experiments [93]. The head phantom was replaced by an artificial torso composed of ribs, muscle, skin, a heart, lungs, and an abdomen fabricated from polyurethane (soft tissue) and epoxy resin (bones). To mimic the cancerous lung tissue, a $1 \times 1 \times 2$ cm^3 artificial cancer made of water, corn flour, gelatin, agar, sodium azide, propylene glycol, and sodium chloride was inserted in the torso phantom. The mixture had the same dielectric properties as lung cancer across the working bandwidth of 1.5–3 GHz. Instead of rotating the table that supported the antenna, as in Figure 9(b), one antenna was adopted with a fixed position, and the phantom was turned in increments of 30° to collect monostatic data in 12 positions. A frequency-domain algorithm was applied to the acquired data to obtain an image. From the reconstructed image that Abbosh's group obtained, the dimension of the "cancerous region" was much bigger than the artificial cancer that was inserted in the torso phantom.

In a later system developed by Abbosh's group, a microwave torso scanner designed in the shape of a doughnut chamber was built with two arrays of 12 antennas [94]. Metamaterial theory was applied to the structure of a conventional Yagi antenna to reduce its size and enable the arrays to be in close proximity. Six human subjects were imaged, and a similarity was found in the intensity of the scattered signals from different healthy cases, indicating the system's feasibility for future clinical trials. Even so, the challenge of imaging the torso is the same as microwave head imaging: it is difficult to balance the penetrating in-body microwave energy and imaging resolution. Thus, better design ideas are necessary before any breakthroughs can be expected in torso and head microwave imaging.

Experimental microwave medical-imaging systems have been reported for a few decades. The designs of such systems progressed from simple and crude to highly precise yet expensive and bulky (such as using a high-dynamic-range VNA) and eventually to more commercially practical and clinically feasible designs. Although the first clinical trials of prototypes occurred more than 10 years ago [11], this technology has not translated into clinical practice, due largely to two technical challenges.

The first is the impedance matching between a human body and an antenna. The dielectric properties of human skin exposed to air significantly vary in the microwave spectrum; hence, human skin acts like a mirror that reflects most of the microwave energy, so only a small portion of the radiated power enters the body. Two popular approaches to resolve this issue involve using a skin-touching antenna and a coupling liquid. In both approaches, the antennas are specially designed to work in a specific scenario. Using a skin-touching antenna may essentially resolve the matching problem; however, the fabrication is challenging. Any air gap between the skin and antenna will cause impedance unmatching. Using a coupling liquid is technically easy, but it only partly relieves the unmatching

problem: The dielectric parameters of the coupling liquid are insufficient to match the skin across a wide spectrum, and the coupling liquid itself is often lossy.

The second challenge involves the tradeoff between penetration depth in the lossy human body and the imaging resolution. Deep penetration requires relatively low microwave frequencies but produces a resolution that is inadequate for clinical diagnosis. These challenges remain, and further developments are needed. As introduced earlier in this section, some additional in-lab clinical trials for breast and brain imaging are underway. We anticipate that these trials will bring additional knowledge to help stimulate future advances so that the difficulties can be overcome.

Nondestructive Testing

NDT technologies are often needed to determine a component of an object or quantitatively measure characteristics. Traditional NDT uses ultrasound or X-ray. Microwave-imaging techniques have been explored in NDT because of their good penetration capability and cost efficiency. Known applications of microwave NDT (for example, see Figure 11) include moisture measurements, wall-thickness measurements, paint-thickness measurements on carbon composites, and quality control (for instance, checking for the presence of seams in composite materials, measuring material permittivity, detecting corrosion and precursor pitting in painted aluminum and steel substrates, finding flaws in spray-on foam insulation, and inspecting the Space Shuttle's acreage heat tiles). In recognition of the growing importance of NDT, an expert committee for microwave and terahertz procedures at the German Society of NDT and a microwave testing committee at the American Society for NDT were founded in 2011 and 2014, respectively. Standardization work has begun along with prototype systems in reflection and through-transmission modes.

Zoughi's research group at the Missouri University of Science and Technology [96] utilized microwave imaging for NDT to investigate a mortar specimen with four different embedded rebars located at a depth of 2 cm, as shown in Figure 12(a). A linear scan was performed above the mortar's surface, denoted by the red arrow in Figure 12(a) and (b). The linear scan was carried out by an antenna located 13.8 cm from the surface and spanning 23 cm along the x direction, with a step size of 0.1 cm. Reflection coefficients were measured and recorded by a VNA from 8.2 to 12.4 GHz. A piecewise SAR algorithm and Wiener-filter–based layered SAR algorithm enabled the production of an image specifying the rebars' position, as depicted in Figure 11(c).

More interesting is a WB microwave camera for real-time 3D imaging developed by Zoughi's group and reported in 2017 [97]. The camera, operating in the 20–30-GHz frequency range, has the potential to perform real-time inspection and diagnosis for NDT, biomedical, and security applications. A monostatic antenna array composed of 16 1D arrays (each including 16 elements that have integrated dual receivers) with a voltage-controlled oscillator (VCO) as the signal source was built on a printed circuit board to transmit and receive signals, as shown in Figure 13(a). The entire system, including the antenna array, switch drivers, analog multiplexer, and other support circuitry (which includes the power regulators and power-sequencing circuitry for the power amplifier), is assembled

with a size of 26 × 21 × 18 cm. The WB microwave camera was tested on a box cutter and scissors inside a laptop bag [Figure 13(b)], successfully imaging them [Figure 13(c)].

Wu and colleagues explored using microwave imaging for flow pipes [98], [99]. Their system contained 16 monopole antennas, eight each for receiving and transmitting; a VNA; and a PC for data acquisition and image reconstruction. The monopoles were arranged with an equal angular spacing around a 130-mm-diameter circle, suitable for an operating range between 2 and 4 GHz. A quasi-3D modeling approach was applied to solve the forward problem for the microwave tomographic system. Two dielectric phantoms were used. The first consisted of a 5-cm-diameter polytetrafluoroethylene (PTFE) cylinder with a permittivity of 2 (similar to oil) located at the center of the imaging area, which had a permittivity of ~1 (similar to gas, which is similar to air), as the background. The second was made up of two 2.5-cm-diameter PTFE cylinders. The images obtained in both cases were sharper when they were reconstructed at 4 GHz than at 2.5 GHz, as illustrated in Figure 14(a) and (b).

Researchers in Moghaddam's group (who were with the University of Michigan and are now at the University of Southern California) created a microwave-imaging system to capture changes in the dielectric constant that results from the application of microwave heating [100], [101], as pictured in Figure 15. Differential-temperature microwave imaging is based on the fact that the dielectric properties of water change as a function of temperature. The researchers used 36 bow-tie patch antennas designed to operate at 915 MHz and a two-port VNA in an isopropyl alcohol and water coupling medium. They imaged a 4-cm water-filled ping-pong ball as it cooled from 55 to 22 °C; the experiment was designed to emulate a thermal-therapy focal spot, with the ultimate goal of improving the monitoring and feedback of thermal treatments, such as thermal ablation and hyperthermia.

Collaborators from the University of Applied Sciences of Southern Switzerland, Centro di Senologia della Svizzera, and the University of Genoa, including Pastorino's research group, developed a multistatic-mode prototype system that was first used for the inspection of dielectric materials, including wooden objects [102], [103]. Images obtained by a linearized Newton method were able to correctly identify defects inside a wood slab. Figure 16(a) shows the experimental setup, and Figure 16(c) presents the reconstructed image. In contrast to Moghaddam's design, which used an array and a number of cables, this system employed a pair of antennas and a rotating table to hold objects. In a later development, plastic extension arms were connected to the antenna arms, which could then be immersed in a coupling medium [104]. Measurements were collected using a VNA. A breast phantom submerged in vegetable oil was placed in the system, and measurements were collected every 22.5° from 2 to 10 GHz, with a 200-MHz increment. Figure 16(b), (d), and (e) shows the experimental setup with the plastic extension arms, breast phantom, and reconstructed image using the inversion algorithm in [105].

Nikolva's group at McMaster University uses 2D planar raster scanning, where one transmitting transverse-EM horn antenna and a bow-tie antenna array with nine elements for reception are moved together along the opposite sides of the imaging domain, as shown in Figure 17(a) [18]. The operating frequency is 3.1 to 10.6 GHz, and a VNA is used for data

acquisition. The system employs holographic imaging and was tested on tissue phantoms and X-shaped metallic targets, as illustrated in Figure 17(b). The reconstructed images of the X-shaped targets, pictured in Figure 17(c), were accurate when accounting for the point-spread function when placed at two different locations. An earlier version of the system reconstructed two spheres made of alginate powder in a glycerine-based phantom [106].

A prototype system developed by Ellumen [107]–[109] uses reflected and transmitted signals in a multistatic mode for microwave NDT. Similar to Pastorino's system, a pair of electronically controlled antennas rotates around an object from zero to 360°, with a 1° accuracy; one antenna serves as the transmitter and the other as the receiver. A wooden, circular tray is placed at the center to support an object and can move in the vertical direction. Microwave measurements can be conducted in the frequency domain when antennas are connected to a VNA and in the time domain when the transmitter antenna is connected to a signal generator and the receiver antenna is connected to an oscillo-scope, as presented in Figure 18(a) and (b).

There are advantages to using movable antennas instead of an array containing many elements, includg avoiding potential unwanted mutual couplings, bypassing the need for a costly and bulky switching-matrix network, and enabling more advanced highgain antennas to be adopted as opposed to a small, simple antenna, such as monopole or dipole. Using the Ellumen system, a complete multistatic scan with both antennas transmitting and receiving from zero to 360° takes a few minutes, depending on the number of signals and the length of each. A phase confocal-imaging algorithm [110] produces an image of the cylindrical object, as shown in Figure 18(c), in which the hollow structure is successfully revealed. The software to control the system consists of a series of steps, as given in Figure 18(d). The software controls the movement of the antennas to any position on the rails by setting the starting and ending positions and the angle increments, enabling multiple measurements to be taken at each location and the average to be calculated to achieve a lower-noise contained signal.

Researchers in LoVetri's group at the University of Manitoba, Canada, developed a microwave-imaging approach using a resonant, air-filled metallic chamber [111], building upon some of their earlier work [112]. Unlike the Pastorino and Ellumen systems, no rotatable antennas or object is present. LoVetri's group used 12 transmit/receive, printed, reconfigurable monopole antennas that could be turned on and off using PIN diodes, in contrast to an earlier system that used 24 antennas [85]. The design also differed from some of the other previously described systems by using a metallic chamber to enable better control of unwanted reflections, potentially facilitating the incorporation of a lossless or low-loss matching medium, and to shield objects from external EM noise. The system was used to image a wooden cube and nylon cylinder, as shown in Figure 19(a) and (b). The reconstructed images, as in Figure 19(c), showed the targets at 1.75 GHz.

Other systems that have been developed are briefly mentioned in the following (the list is not inclusive). Liu's group at Duke University, North Carolina, created a system that uses two dipoles with data acquisition from a VNA to reconstruct clay balls placed in water [113]. A system by Bolomey's group at the French National Center for Scientific Research

employs a planar microwave camera at 2.45 GHz and two horn antennas to image a breast phantom [114]. Additionally, a system was developed by Jofre's group at the University of Catalunya, Spain, using two UWB antennas, one of them on a rotary stage and the other on a fixed platform, to image cylindrical objects [115], [116] and clay balls [117]. Villarino's group at the Universitat Rovira i Virgili, Italy, developed two systems to image a rod in a cylindrical tank: the first incorporating a VNA and one antenna [118] and the other employing a pulse generator and sampler converter using two antennas [119]. Another system was developed by Mase and colleagues at Toyohashi University of Technology, Japan, using two Vivaldi antennas and an oscilloscope to image a breast phantom inside a tank, with the best results obtained using a matching liquid of cooking oil [120]. Yet another system was devised by Nanyang Technological University and Low's group using two antennas and an oscilloscope to image breast phantoms [121].

Table 3 compares NDT systems selected from those described previously. The comparison highlights the number and type of antennas used, frequencies of operation, hardware, and inclusion of a coupling liquid. Several systems use mechanical devices to rotate the antenna elements. Some systems mimic a raster scan that is common in X-ray imaging and have a sole transmitter and sole receiver, whereas others incorporate many antenna elements.

Through-the-Wall Imaging

Through-the-wall imaging is one of the most important microwave technologies to emerge in recent years. Such systems provide enhanced situational awareness in a variety of civilian and military applications. They not only detect the presence of objects behind walls but also provide information concerning each target's location, motion, size, and backscattering cross section. Compared with traditional radar applications, through-the-wall radar imaging faces challenges, such as unknown dielectric characteristics and the thickness of the wall, signal attenuation in the wall, and unknown target movement.

Many approaches have tested through-the-wall radar-imaging techniques. The most widely used is the WB or UWB radar mechanism, which contains an antenna array or one antenna measuring at multiple locations to form a synthetic aperture [122]–[128]. The bandwidth typically ranges from a few hundred megahertz to several gigahertz. All the antenna elements in the array (or one antenna at every location) measure backscattered signals, which are compensated against their time delaying and weighting and synthesized to produce an image. An example of this is provided in Figure 20. Another example concerns a device developed by Akduman's group [129]; it uses a pair of horn antennas operating between 0.8 and 5 GHz. The pair works in a bistatic mode and moves along the wall to collect the signal from different positions. An experiment with the system was performed in a large anechoic chamber. An image of objects behind a wall was reconstructed by processing the acquired data with an inverse-scattering algorithm (microwave tomography). A third approach uses a frequency-modulated continuous-wave radar [130], [131] or a step-frequency continuous-wave (SFCW) radar [132]. This technique detects a Doppler frequency shift caused by the target's motion or vital signs, such as a heartbeat and breath. Other approaches, including the time-reversal technique [133] and tomographic inverse-

scattering method [134], have been used in through-the-wall microwave imaging, which has achieved commercial success.

Security Screening

Microwave-imaging techniques have been proposed to detect concealed weapons at major transportation hubs to replace the conventional X-ray screening method, since they may present fewer potential health risks, especially for pregnant women and infants. Microwave-imaging systems' nonionizing characteristic and low cost increase the likelihood of their adoption in this area.

The systems detect a high frequency that is reflected by human skin and passes through most fabrics, making it possible to reconstruct the 3D shape of a person and any metal, which microwave cannot penetrate, that he or she may possess. Likely due to hardware restrictions, there are only a limited number of studies in this area. In 2001, Sheen and colleagues at the Pacific Northwest National Laboratory, Richland, Washington, reported the first 3D whole-body imaging using the principles of microwave holography [135]. The goal was to achieve real-time imaging (on the order of 3 to 10 s) for concealed-weapon detection. A prototype imaging system utilizing a 27–33 GHz linear sequentially switched array was developed and tested for locating a hidden explosive. Later, microwave holographic-imaging technology was expanded by Sheen and colleagues for multiple applications [136] with different frequency ranges: 3D imaging of a helicopter using an impulse radar, operating at 1–5 GHz; imaging a Bradley Fighting Vehicle, operating at 8–12 GHz; 3D ground-penetrating-radar imaging of twin waste-storage tanks, operating at 200–400 MHz; and detecting concealed weapons attached to a mannequin, operating at 40–60 GHz and 10–20 GHz during different tests.

In 2011, Zhuge et al. [137], [138] attempted to use the UWB method with a multiple input/multiple output (MIMO) array to deliver high-resolution 3D images for concealed-weapon detection in quasi-real time. The system combined UWB, MIMO, and SAR technology. The MIMO array consisted of four antipodal Vivaldi antennas as transmitters and eight such antennas as receivers, operating at a center frequency of 11.15 GHz and 150% fractional bandwidth (2.8–19.5 GHz). Elements in the MIMO array were connected to a network analyzer through a multiport switch, and the entire array was mounted on a computer-controlled mechanical scanner, enabling azimuth and elevation scans to form an SA for 3D volumetric imaging, as shown in Figure 21(b). When a weapon attached to a 1.8-m-high, 0.5-m-wide mannequin (covered with aluminum foil to mimic a shield for the weapon) was exposed to the MIMO array, a 3D image of was achieved by processing the received data. It was possible to determine the shape of the weapon attached to the mannequin, as detailed in Figure 21(c).

Due to technical progress in RF manufacturing and cost reductions, mm-wave [139], [140] and terahertz [141] imaging have been considered for security applications. The use of a shorter wavelength leads to better range resolution. In [139], an active mm-wave SFCW radar operating at 59–61 GHz was tested to image an aluminum-foil–wrapped toy gun covered with cloth. A 2D scan composed of 30 × 18 locations with a 0.02-m spacing in the

vertical and horizontal directions was performed. The imaging results validated the idea of using mm-wave–imaging radar systems for concealed-weapon detection. In contrast, terahertz imaging uses even higher frequencies to achieve greater spatial resolution. In [141], Knipper et al. compared the effect of using 0.35 and 0.85 THz for a passive security camera to detect a weapon beneath clothes. Terahertz imaging was found to be influenced by signal absorption in fabric, especially wet clothes, causing a 0.85-THz band to be a less desirable option than 0.35 THz, although 0.85 THz provided better resolution.

Outlook

During the past few decades, microwave near-field imaging has experienced conceptualizations, theoretical analyses, simulation tests, and experimental validation. Due to technical developments in hardware manufacturing and software, many prototype systems for a variety of applications have emerged since the early 2000s. Microwave scientists and engineers are working toward optimizing current prototypes for production and widespread use.

Bulky and expensive signal-recording tools, including VNAs and oscilloscopes, are being replaced by more compact, cost-effective, and customized instruments, such as high-speed ADCs and FPGAs. This trend will enable current prototypes to lead the way toward the first commercial microwave-imaging product. In addition, the growth of this technology will extend from research institutions and academia to industrial research and development. Additional clinical trials are necessary to unite the microwave-engineering and medical communities and collect important clinical evidence to prove the techniques' effectiveness. Developments that reduce system cost and size and increase ease of use for patients are necessary. It can be expected that more applications of microwave-imaging techniques will emerge in the not-too-distant future and lead to benefits for individuals and society.

References

[1]. Larsen LE and Jacobi JH, "Microwave interrogation of dielectric targets. Part I: By scattering parameters," Med. Phys, vol. 5, no. 6, pp. 500–508, 1978. doi: 10.1118/1.594460. [PubMed: 732773]

[2]. Larsen LE and Jacobi JH, "Microwave interrogation of dielectric targets. Part II: By microwave time delay spectroscopy," Med. Phys, vol. 5, no. 6, pp. 509–513, 1978. doi: 10.1118/1.594461. [PubMed: 732774]

[3]. Larsen LE and Jacobi JH, Eds., Medical Applications of Microwave Imaging. New York: IEEE Press, 1986.

[4]. Pichot C, Jofre L, Peronnet G, and Bolomey J-C, "Active microwave imaging of inhomogeneous bodies," IEEE Trans. Antennas Propag, vol. 33, no. 4, pp. 416–425, 4. 1985. doi: 10.1109/TAP.1985.1143603.

[5]. Bolomey JC and Pichot C, "Microwave tomography: From theory to practical imaging systems," Int. J. Imaging Syst. Technol, vol. 2, no. 2, pp. 144–156, 1990. doi: 10.1002/ima.1850020210.

[6]. Franchois A, Joisel A, Pichot C, and Bolomey J-C, "Quantitative microwave imaging with a 2.45-GHz planar microwave camera," IEEE Trans. Med. Imag, vol. 17, no. 4, pp. 550–561, 8. 1998. doi: 10.1109/42.730400.

[7]. Schaller G, "On the imaging of hot spots using correlation radiometers and a circular aperture," IEEE Trans. Microw. Theory Techn, vol. 37, no. 8, pp. 1210–1216, 8. 1989. doi: 10.1109/22.31080.

[8]. Carr KL, “Microwave radiometry: Its importance to the detection of cancer,” IEEE Trans. Microw. Theory Techn, vol. 37, no. 12, pp. 1862–1869, 12. 1989. doi: 10.1109/22.44095.

[9]. Mouty S, Bocquet B, Ringot R, Rocourt N, and Devos P, “Microwave radiometric imaging for the characterization of breast tumors,” Eur. Phys. J., Appl. Phys, vol. 10, no. 1, pp. 73–78, 2000. doi: 10.1051/epjap:2000121.

[10]. Carr KL, Cevasco P, Dunlea P, and Shaeffer J, “Radiometric sensing: An adjuvant to mammography to determine breast biopsy,” in Proc. IEEE MTT-S Int. Microwave Symp. Dig, 6 2000, pp. 929–932. doi: 10.1109/MWSYM.2000.863509.

[11]. Meaney PM, Fanning MW, Li D, Poplack SP, and Paulsen KD, “A clinical prototype for active microwave imaging of the breast,” IEEE Trans. Microw. Theory Techn, vol. 48, no. 11, pp. 1841–1853, 11. 2000. doi: 10.1109/22.883861.

[12]. Fear EC, Hagness SC, Meaney PM, Okoniewksi M, and Stuchly MA, “Enhancing breast tumor detection with near-field imaging,” IEEE Microw. Mag, vol. 3, no. 1, pp. 48–56, 3. 2002. doi: 10.1109/6668.990683.

[13]. Nikolova NK, “Microwave imaging for breast cancer,” IEEE Microw. Mag, vol. 12, no. 7, pp. 78–94, 12. 2011. doi: 10.1109/MMM.2011.942702.

[14]. Fhager A, Candefjord S, Elam M, and Persson M, “Microwave diagnostics ahead,” IEEE Microw. Mag, vol. 19, no. 3, pp. 78–90, 5 2018. doi: 10.1109/MMM.2018.2801646.

[15]. Steinberg BD and Subbaram HM, Microwave Imaging Technique. New York: Wiley, 1991.

[16]. Pastorino M, Microwave Imaging. Hoboken, NJ: Wiley, 2010.

[17]. Nikolova NK, “Microwave biomedical imaging,” in Wiley Encyclopedia of Electrical and Electronics Engineering, Webster JG, Ed. Hoboken, NJ: Wiley, 2014, pp. 1–22.

[18]. Amineh RK, McCombe J, Khalatpour A, and Nikolova NK, “Microwave holography using measured point-spread functions,” IEEE Trans. Instrum. Meas, vol. 64, no. 2, pp. 403–417, 2. 2015. doi: 10.1109/TIM.2014.2347652.

[19]. Kwon S and Lee S, “Recent advances in microwave imaging for breast cancer detection,” Int. J. Biomed. Imaging, vol. 2016, art. ID 5054912, pp. 1–26, 2016. doi: 10.1155/2016/5054912.

[20]. Conceição RC, Mohr JJ, and O’Halloran M, Eds., An Introduction to Microwave Imaging for Breast Cancer Detection. New York: Springer-Verlag, 2016.

[21]. Nikolova NK, Introduction to Microwave Imaging. Cambridge, U.K.: Cambridge Univ. Press, 2017.

[22]. O’Loughlin D, O’Halloran MJ, Moloney BM, Glavin M, Jones E, and Elahi MA, “Microwave breast imaging: Clinical advances and remaining challenges,” IEEE Trans. Biomed. Eng, vol. 65, no. 11, pp. 2580–2590, 2. 2018. doi: 10.1109/TBME.2018.2809541. [PubMed: 29993488]

[23]. Yang R et al., High-Resolution Microwave Imaging. Singapore: Springer-Verlag, 2018.

[24]. Sugitani T et al., “Complex permittivities of breast tumor tissues obtained from cancer surgeries,” Appl. Phys. Lett, vol. 104, no. 25, pp. 253702–253702–5, 6 2014. doi: 10.1063/1.4885087.

[25]. Meaney PM et al., “Initial clinical experience with microwave breast imaging in women with normal mammography,” Acad. Radiol, vol. 14, no. 2, pp. 207–218, 2. 2007. doi: 10.1016/j.acra.2006.10.016. [PubMed: 17236994]

[26]. Golnabi AH, Meaney PM, Epstein NR, and Paulsen KD, “Microwave imaging for breast cancer detection: Advances in three-dimensional image reconstruction,” in Proc. 33rd Annu. Int. Conf. IEEE Engineering in Medicine and Biology Society, Aug-Sep 2011, pp. 5730–5733. doi: 10.1109/IEMBS.2011.6091418.

[27]. Epstein NR, Meaney PM, and Paulsen KD, “3D parallel-detection microwave tomography for clinical breast imaging,” Rev. Sci. Instrum, vol. 85, no. 12, p. 124,704, 12. 2014. doi: 10.1063/1.4901936.

[28]. Meaney PM et al., “Microwave imaging for neoadjuvant chemotherapy monitoring: Initial clinical experience,” Breast Cancer Res, vol. 15, no. 2, p. R35, 2013. doi: 10.1186/bcr3418. [PubMed: 23621959]

[29]. Li X, Bond E, Van Veen B, and Hagness S, “An overview of ultrawideband microwave imaging via space-time beamforming for early-stage breast-cancer detection,” IEEE Trans. Antennas Propag, vol. 47, pp. 19–34, 2. 2005. doi: 10.1109/MAP.2005.1436217.

[30]. Klemm M, Craddock I, Leendertz J, Preece A, and Benjamin R, "Experimental and clinical results of breast cancer detection using UWB microwave radar," in Proc. IEEE Antennas and Propagation Society Int. Symp, 7 2008, pp. 1–4. doi: 10.1109/APS.2008.4619673.

[31]. Klemm M et al., "Clinical trials of a UWB imaging radar for breast cancer," in Proc. 4th European Conf. Antennas and Propagation (EuCAP), 4. 2010, pp. 1–4.

[32]. Klemm M, Leendertz JA, Gibbins D, Craddock IJ, Preece A, and Benjamin R, "Microwave radar-based differential breast cancer imaging: Imaging in homogeneous breast phantoms and low contrast scenarios," IEEE Trans. Antennas Propag, vol. 58, no. 7, pp. 2337–2344, 7 2010. doi: 10.1109/TAP.2010.2048860.

[33]. Klemm M et al., "Development and testing of a 60-element UWB conformal array for breast cancer imaging," in Proc. 5th European Conf. Antennas and Propagation (EuCAP), 4. 2011, pp. 3077–3079.

[34]. Henriksson T et al., "Clinical trials of a multistatic UWB radar for breast imaging," in Proc. Loughborough Antennas and Propagation Conf, 2011, pp 1–4. doi: 10.1109/LAPC.2011.6114004.

[35]. Preece AW, Craddock I, Shere M, Jones L, and Winton HL, "MARIA M4: Clinical evaluation of a prototype ultrawideband radar scanner for breast cancer detection," J. Med. Imaging, vol. 3, no. 3, pp. 033502–1–033502–7, 7 2016. doi: 10.1117/1.JMI.3.3.033502.

[36]. Bourqui J, Okoniewski M, and Fear EC, "Balanced antipodal Vivaldi antenna with dielectric director for near-field microwave imaging," IEEE Trans. Antennas Propag, vol. 58, no. 7, pp. 2318–2326, 7 2010. doi: 10.1109/TAP.2010.2048844.

[37]. William TC, Bourqui J, Cameron TR, Okoniewski M, and Fear EC, "Laser surface estimation for microwave breast imaging systems," IEEE Trans. Biomed. Eng, vol. 58, no. 5, pp. 1193–1199, 5 2011. doi: 10.1109/TBME.2010.2098406. [PubMed: 21147590]

[38]. Fear EC, Bourqui J, Curtis C, Mew D, Docktor B, and Romano C, "Microwave breast imaging with a monostatic radar-based system: A study of application to patients," IEEE Trans. Microw. Theory Techn, vol. 61, no. 5, pp. 2119–2128, 5 2013. doi: 10.1109/TMTT.2013.2255884.

[39]. Li X and Hagness SC, "A confocal microwave imaging algorithm for breast cancer detection," IEEE Microw. Compon. Lett, vol. 11, no. 3, pp. 130–132, 3. 2001. doi: 10.1109/7260.915627.

[40]. Bourqui J, Kuhlmann M, Kurrant DJ, Lavoie BR, and Fear EC, "Adaptive monostatic system for measuring microwave reflections from the breast," Sensors, vol. 18, no. 5, p. 1340, 5 2018. doi: 10.3390/s18051340.

[41]. Bourqui J and Fear EC, "System for bulk dielectric permittivity estimation of breast tissues at microwave frequencies," IEEE Trans. Microw. Theory Techn, vol. 64, no. 9, pp. 3001–3009, 9. 2016. doi: 10.1109/TMTT.2016.2586486.

[42]. Zeng X, Fhager A, Linner P, Persson M, and Zirath H, "Experimental investigation of the accuracy of an ultrawideband time-domain microwave-tomographic system," IEEE Trans. Instrum. Meas, vol. 60, no. 12, pp. 3939–3949, 12. 2011. doi: 10.1109/TIM.2011.2141250.

[43]. Zeng X, Fhager A, Persson M, Linner P, and Zirath H, "Accuracy evaluation of ultrawideband time domain systems for microwave imaging," IEEE Trans. Antennas Propag, vol. 59, no. 11, pp. 4279–4285, 11. 2011. doi: 10.1109/TAP.2011.2164174.

[44]. Zeng X, Fhager A, He Z, Persson M, Linner P, and Zirath H, "Development of a time domain microwave system for medical diagnostics," IEEE Trans. Instrum. Meas, vol. 63, no. 12, pp. 2931–2939, 12. 2014. doi: 10.1109/TIM.2014.2326277.

[45]. Zhurbenko V, Rubaek T, Krozer V, and Meincke P, "Design and realization of a microwave three-dimensional imaging system with application to breast-cancer detection," IET Microw. Antennas Propag, vol. 4, no. 12, pp. 2200–2211, 12. 2010. doi: 10.1049/ietmap.2010.0106.

[46]. Jensen PD, Rubaek T, Mohr JJ, and Zhurbenko V, "Nonlinear 3-D microwave imaging for breast-cancer screening: Log, phase and log-phase formulation," in Proc. Loughborough Antennas and Propagation Conf, 2011, pp. 1–4. doi: 10.1109/LAPC.2011.6114124.

[47]. Porter E, Santorelli A, Coates M, and Popovic M, "An experimental system for time-domain microwave breast imaging," in Proc. 5th European Conf. Antennas and Propagation (EuCAP), 4. 2011, pp. 2906–2910.

[48]. Popovic M and Kanj H, “Microwave scanning system and miniaturized microwave antenna,” U.S. Patent 8 089 417, 1. 3, 2012.

[49]. Porter E, Kirshin E, Santorelli A, Coates M, and Popovic M, “Time-domain multistatic radar system for microwave breast screen,” IEEE Antennas Wireless Propag. Lett, vol. 12, pp. 229–232, 2013. doi: 10.1109/LAWP.2013.2247374.

[50]. Porter E, Santorelli A, and Popovic M, “Time-domain microwave radar applied to breast imaging: Measurement reliability in a clinical setting,” Prog. Electromag. Res, vol. 149, pp. 119–132, 2014. doi: 10.2528/PIER14080503.

[51]. Porter E, Coates M, and Popovic M, “An early clinical study of time-domain microwave radar for breast health monitoring,” IEEE Trans. Biomed. Eng, vol. 63, no. 3, pp. 530–539, 3. 2016. doi: 10.1109/TBME.2015.2465867. [PubMed: 26259214]

[52]. Porter E, Bahrami H, Santorelli A, Gosselin B, Rusch LA, and Popovic M, “A wearable microwave antenna array for time-domain breast tumor screening,” IEEE Trans. Med. Imag, vol. 35, no. 6, pp. 1501–1509, 6 2016. doi: 10.1109/TMI.2016.2518489.

[53]. Porter E, Duff K, Popović M, and Coates M., “Investigation of time-domain microwave radar with breast clinic patients,” in Proc. 10th Euro. Conf. Antennas and Propagation, Davos, Switzerland, 4. 2016, pp. 1–3. doi: 10.1109/EuCAP.2016.7481765.

[54]. Tobon Vasques JA, Vipiana F, Casu MR, Vacca M, and Pulimeno A, “Microwave imaging for early breast cancer detection: Experimental testing of a low-cost portable system,” in Proc. IEEE Int. Symp. Antennas and Propagation (APSURSI), 7 2016, pp. 1479–1480. doi: 10.1109/APS.2016.7696446.

[55]. Tobon Vasques JA, Vipiana F, Casu MR, Vacca M, and Pulimeno A, “Experimental testing of a low-cost microwave imaging system for early breast cancer detection,” in Proc. 10th European Conf. Antennas and Propagation (EuCAP), 4. 2016, pp. 1–3. doi: 10.1109/EuCAP.2016.7481763.

[56]. Casu MR et al., “A cots-based microwave imaging system for breast cancer detection,” IEEE Trans. Biomed. Circuits Syst, vol. 11, no. 4, pp. 804–814, 8. 2017. doi: 10.1109/TBCAS.2017.2703588. [PubMed: 28727561]

[57]. Song H et al., “Detectability of breast tumor by a hand-held impulse-radar detector: Performance evaluation and pilot clinical study,” Sci. Rep, vol. 7, no. 1, p. 16,353, 11. 2017. doi: 10.1038/s41598-017-16617-6. [PubMed: 28154412]

[58]. Son SH, Simonov N, Kim HJ, Lee JM, and Jeon SI, “Preclinical prototype development of a microwave tomography system for breast cancer detection,” ETRI J, vol. 32, no. 6, pp. 901–910, 2010. doi: 10.4218/etrij.10.0109.0626.

[59]. Kwon KC et al., “Microwave tomography analysis system for breast tumor detection,” J. Med. Syst, vol. 36, no. 3, pp. 1757–1767, 2012. doi: 10.1007/s10916-010-9635-4. [PubMed: 21210189]

[60]. Lee J, Son S, Kim B, Choi H, and Jeon S, “Animal testing using 3d microwave tomography system for breast cancer detection,” in e-Health: For Continuity of Care, Lovis C, Séroussi B, Hasman A, Pape-Haugaard L, Saka O, and Andersen SK, Eds. Amsterdam, The Netherlands: IOS Press, 2014, pp. 491–495.

[61]. Yang F et al., “A large-scale clinical trial of radar-based microwave breast imaging for Asian women: Phase I,” in Proc. IEEE Int. Symp. Antennas and Propagation, San Diego, CA, 7 2017, pp. 781–783. doi: 10.1109/APUSNCURSINRSM.2017.8072433.

[62]. Kuwahara Y, Miura S, Nishina Y, Mukumoto K, Ogura H, and Sakahara H, “Clinical test of microwave mammography,” in Proc. IEEE Antennas and Propagation Society Int. Symp, Orlando, FL, 7 2013, pp. 2028–2029. doi: 10.1109/APS.2013.6711672.

[63]. Kuwahara Y, “Microwave imaging for early breast cancer detection,” in New Perspectives in Breast Imaging, Malik AM, Ed. London: IntechOpen, 10. 2017.

[64]. Semenov SY et al., “Dielectrical spectroscopy of canine myocardium during acute ischemia and hypoxia at frequency spectrum from 100 kHz to 6 GHz,” IEEE Trans. Med. Imag, vol. 21, no. 6, pp. 703–707, 6 2002. doi: 10.1109/TMI.2002.800590.

[65]. Lin JC and Clark MJ, “Microwave imaging of cerebral edema,” Proc. IEEE, vol. 70, no. 5, pp. 523–524, 5 1982. doi: 10.1109/PROC.1982.12341.

[66]. Semenov SY and Corfield DR, “Microwave tomography for brain imaging: Feasibility assessment for stroke detection,” Int. J. Antennas Propag, vol. 2008, art. ID 254830, 2008. doi: 10.1155/2008/254830.

[67]. Trefna H and Persson M, “Antenna array design for brain monitoring,” in Proc. IEEE Antennas and Propagation Society Int. Symp, 7 2008, pp. 1–4. doi: 10.1109/APS.2008.4619683.

[68]. Souvorov AE et al., “Microwave tomography: A two-dimensional Newton iterative scheme,” IEEE Trans. Microw. Theory Techn, vol. 46, no. 11, pp. 1654–1659, 11. 1998. doi: 10.1109/22.734548.

[69]. Persson M et al., “Microwave-based stroke diagnosis making global prehospital thrombolytic treatment possible,” IEEE Trans. Biomed. Eng, vol. 61, no. 11, pp. 2806–2817, 11. 2014. doi: 10.1109/TBME.2014.2330554. [PubMed: 24951677]

[70]. Candefjord S et al., “Microwave technology for detecting traumatic intracranial bleedings: Tests on phantom of subdural hematoma and numerical simulations,” Med. Biol. Eng. Comput, vol. 55, no. 8, pp. 1177–1188, 2017. doi: 10.1007/s11517-016-1578-6. [PubMed: 27738858]

[71]. Ljungqvist J, Candefjord S, Persson M, Jönsson L, Skoglund T, and Elam M, “Clinical evaluation of a microwave-based device for detection of traumatic intracranial hemorrhage,” J. Neurotrauma, vol. 34, no. 13, pp. 2176–2182, 2017. doi: 10.1089/neu.2016.4869. [PubMed: 28287909]

[72]. Mustafa S, Mohammed B, and Abbosh A, “Novel preprocessing techniques for accurate microwave imaging of human brain,” IEEE Antennas Wireless Propag. Lett, vol. 12, pp. 460–463, 2013. doi: 10.1109/LAWP.2013.2255095.

[73]. Ireland D, Bialkowski K, and Abbosh A, “Microwave imaging for brain stroke detection using Born iterative method,” IET Microw., Antennas Propag, vol. 7, no. 11, pp. 909–915, 5 2013. doi: 10.1049/iet-map.2013.0054.

[74]. Mohammed BJ, Abbosh AM, Mustafa S, and Ireland D, “Microwave system for head imaging,” IEEE Trans. Instrum. Meas, vol. 63, no. 1, pp. 117–123, 1. 2014. doi: 10.1109/TIM.2013.2277562.

[75]. Mobashsher AT, Abbosh AM, and Wang Y, “Microwave system to detect traumatic brain injuries using compact unidirectional antenna and wideband transceiver with verification on realistic head phantom,” IEEE Trans. Microw. Theory Techn, vol. 62, no. 9, pp. 1826–1836, 9. 2014. doi: 10.1109/TMTT.2014.2342669.

[76]. Mobashsher AT and Abbosh AM, “Compact 3-D slot-loaded folded dipole antenna with unidirectional radiation and low impulse distortion,” IEEE Trans. Antennas Propag, vol. 64, no. 7, pp. 3245–3250, 7 2016. doi: 10.1109/TAP.2016.2560909.

[77]. Mobashsher AT and Abbosh AM, “On-site rapid diagnosis of intracranial hematoma using portable multi-slice microwave imaging system,” Sci. Rep, vol. 6, p. 37,620, 11. 2016. doi: 10.1038/srep37620.

[78]. Touriner P-H et al., “Microwave tomography for brain stroke imaging,” in Proc. IEEE Int. Symp. Antennas and Propagation USNC/URSI Nat. Radio Science Meeting, 7 2017, pp. 29–30. doi: 10.1109/APUSNCURSINRSM.2017.8072057.

[79]. Tournier P-H et al., “Numerical modeling and high-speed parallel computing: New perspectives on tomographic microwave imaging for brain stroke detection and monitoring,” IEEE Antennas Propag. Mag, vol. 59, no. 5, pp. 98–110, 10. 2017. doi: 10.1109/MAP.2017.2731199.

[80]. Salvador SM, Fear EC, Okoniewski M, and Matyas JR, “Microwave imaging of the knee: On sensitivity, resolution and multiple tears detection,” in Proc. 13th Int. Symp. Antenna Technology and Applied Electromagnetics and the Canadian Radio Science Meeting, 2. 2009, pp. 1–4. doi: 10.1109/ANTEMURSI.2009.4805109.

[81]. Salvador SM, Fear EC, Okoniewski M, and Matyas JR, “Exploring joint tissues with microwave imaging,” IEEE Trans. Microw. Theory Techn, vol. 58, no. 8, pp. 2307–2313, 8. 2010. doi: 10.1109/TMTT.2010.2052662.

[82]. Salvador SM, Fear EC, Okoniewski M, and Matyas JR, “Microwave imaging of the knee: Application to ligaments and tendons,” in Proc. IEEE MTT-S Int. Microwave Symp. Dig, 7 2009, pp. 1437–1440. doi: 10.1109/MWSYM.2009.5165977.

[83]. Semenov S et al., "Microwave tomography of extremities: 2. Functional fused imaging of flow reduction and simulated compartment syndrome," Phys. Med. Biol, vol. 56, no. 7, pp. 2019–2030, 2011. doi: 10.1088/0031-9155/56/7/007. [PubMed: 21364266]

[84]. Semenov S et al., "Microwave tomography of extremities: 1. Dedicated 2d system and physiological signatures," Phys. Med. Biol, vol. 56, no. 7, pp. 2005–2017, 2011. doi: 10.1088/0031-9155/56/7/006. [PubMed: 21364265]

[85]. Ostadrahimi M, Mojabi P, Zakaria A, LoVetri J, and Shafai L, "Enhancement of gauss-newton inversion method for biological tissue imaging," IEEE Trans. Microw. Theory Techn, vol. 61, no. 9, pp. 3424–3434, 2013. doi: 10.1109/TMTT.2013.2273758.

[86]. Golnabi AH, Meaney PM, Geimer S, Zhou T, and Paulsen KD, "Microwave tomography for bone imaging," in Proc. IEEE Int. Symp. Biomedical Imaging: From Nano to Macro, Mar-Apr 2011, pp. 956–959. doi: 10.1109/ISBI.2011.5872561.

[87]. Meaney PM et al., "Clinical microwave tomographic imaging of the calcaneus: A first-in-human case study of two subjects," IEEE Trans. Biomed. Eng, vol. 59, no. 12, pp. 3304–3313, 12. 2012. doi: 10.1109/TBME.2012.2209202. [PubMed: 22829363]

[88]. Chand K, Mehta P, Beetner DG, Zoughi R, and Stoecker WV, "Microwave reflectometry as a novel diagnostic method for detection of skin cancers," in Proc. IEEE Instrumentation and Measurement Technology Conf, 5 2005, pp. 1425–1428. doi: 10.1109/IMTC.2005.1604385.

[89]. Mehta P, Chand K, Narayanswamy D, Beetner DG, Zoughi R, and Stoecker WV, "Microwave reflectometry as a novel diagnostic tool for detection of skin cancers," IEEE Trans. Instrum. Meas, vol. 55, no. 4, pp. 1309–1316, 8. 2006. doi: 10.1109/TIM.2006.876566.

[90]. Taeb A, Gigoyan S, and Safavi-Naeini S, "Millimetre-wave waveguide reflectometers for early detection of skin cancer," IET Microw. Antennas Propag, vol. 7, no. 14, pp. 1182–1186, 11. 2013. doi: 10.1049/iet-map.2013.0189.

[91]. Topfer F, Dudorov S, and Oberhammer J, "Millimeter-wave near-field probe designed for high-resolution skin cancer diagnosis," IEEE Trans. Microw. Theory Techn, vol. 63, no. 6, pp. 2050–2059, 6 2015. doi: 10.1109/TMTT.2015.2428243.

[92]. Gao Y and Zoughi R, "Millimeter wave reflectometry and imaging for noninvasive diagnosis of skin burn injuries," IEEE Trans. Instrum. Meas, vol. 66, no. 1, pp. 77–84, 1. 2017. doi: 10.1109/TIM.2016.2620778.

[93]. Zamani A, Rezaeieh SA, and Abbosh AM, "Lung cancer detection using frequency-domain microwave imaging," Electron. Lett, vol. 51, no. 10, pp. 740–741, 5 2015. doi: 10.1049/el.2015.0230.

[94]. Rezaeieh SA, Zamani A, Bialkowski KS, and Abbosh AM, "Novel microwave torso scanner for thoracic fluid accumulation diagnosis and monitoring," Sci. Rep, vol. 7, no. 1, p. 304, 3. 2017. doi: 10.1038/s41598-017-00436-w. [PubMed: 28331176]

[95]. Hinken J, "Microwave testing (μT): An overview," FI Test-und Messtechnik GmbH, Magdeburg, Germany, 7 2016. [Online]. Available: http://fitm.de/wp-content/uploads/2017/07/N38e-Microwave-Testing_An-Overview.pdf

[96]. Fallahpour M, Case JT, Ghasr MT, and Zoughi R, "Piecewise and wiener filter-based SAR techniques for monostatic microwave imaging of layered structures," IEEE Trans. Antennas Propag, vol. 62, no. 1, pp. 282–294, 1. 2014. doi: 10.1109/TAP.2013.2287024.

[97]. Ghasr MT, Horst MJ, Dvorsky MR, and Zoughi R, "Wideband microwave camera for real-time 3-D imaging," IEEE Trans. Antennas Propag, vol. 65, no. 1, pp. 258–268, 1. 2017. doi: 10.1109/TAP.2016.2630598.

[98]. Wu Z, McCann H, Davis L, Hu J, Fontes A, and Xie C, "Microwave-tomographic system for oil- and gas-multiphase-flow imaging," Meas. Sci. Technol, vol. 20, no. 10, pp. 1–8, 2009. doi: 10.1088/0957-0233/20/10/104026. [PubMed: 20463843]

[99]. Wu Z, "Developing a microwave tomographic system for multi phase flow imaging: Advances and challenges," Trans. Inst. Meas. Control, vol. 37, no. 6, pp. 760–768, 2015. doi: 10.1177/0142331214546523.

[100]. Haynes M, Stang J, and Moghaddam M, "Microwave breast imaging system prototype with integrated numerical characterization," Int. J. Biomed. Imaging, vol. 2012, 2012. doi: 10.1155/2012/706365.

[101]. Haynes M, Stang J, and Moghaddam M, “Real-time microwave imaging of differential temperature for thermal therapy monitoring,” IEEE Trans. Biomed. Eng, vol. 61, no. 6, pp. 1787–1796, 6 2014. doi: 10.1109/TBME.2014.2307072. [PubMed: 24845289]

[102]. Salvade A, Pastorino M, Monleone R, Bozza G, and Randazzo A, “A new microwave axial tomograph for the inspection of dielectric materials,” IEEE Trans. Instrum. Meas, vol. 58, no. 7, pp. 2072–2079, 7 2009. doi: 10.1109/TIM.2009.2015521.

[103]. Randazzo A, Pastorino M, Salvade A, Monleone R, Maffongelli M, and Lanini M, “A multistatic tomographic approach to microwave imaging of dielectric targets,” in Proc. 5th European Conf. Antennas and Propagation (EUCAP), 4. 2011, pp. 2790–2794.

[104]. Maffongelli M et al., “Preliminary test of a prototype of microwave axial tomograph for medical applications,” in Proc. Int. Symp. Medical Measurements and Applications (MeMeA), 5 2015, pp. 46–51. doi: 10.1109/MeMeA.2015.7145170.

[105]. Bozza G, Estatico C, Massa A, Pastorino M, and Randazzo A, “Short-Range image-based method for the inspection of strong scatterers using microwaves,” IEEE Trans. Instrum. Meas, vol. 56, no. 4, pp. 1181–1188, 8. 2007. doi: 10.1109/TIM.2007.900127.

[106]. Amineh RK, Khalatpour A, Xu H, Baskharoun Y, and Nikolova N, “Three-dimensional near-field microwave holography for tissue imaging,” Int. J. Biomed. Imag, vol. 2012, art ID 291494, pp. 1–11, 2012. doi: 10.1155/2012/291494.

[107]. Shao W, Edalati A, McCollough TR, and McCollough WJ, “Experimental microwave near-field detection with moveable antennas,” in Proc. IEEE Int. Symp Antennas and Propagation and USNC/URSI Nat. Radio Science Meeting, 7 2017, pp. 2387–2388. doi: 10.1109/APUSNCURSINRSM.2017.8073236.

[108]. Shao W, Edalati A, McCollough TR, and McCollough WJ, “A time-domain measurement system for UWB microwave imaging,” IEEE Trans. Microw. Theory Techn, vol. 66, no. 5, pp. 2265–2275, 2. 2018. doi: 10.1109/TMTT.2018.2801862.

[109]. McCollough WJ, McCollough TR, Shao W, Edalati A, and Leslie JR, “Microwave imaging device,” U.S. Patent 9 869 641, 1. 16, 2018.

[110]. Shao W, Edalati A, McCollough TR, and McCollough WJ, “A phase confocal method for near-field microwave imaging,” IEEE Trans. Microw. Theory Techn, vol. 65, no. 7, pp. 2508–2515, 7 2017. doi: 10.1109/TMTT.2016.2637930.

[111]. Asefi M, Zakaria A, and LoVetri J, “Microwave imaging using normal electric-field components inside metallic resonant chambers,” IEEE Trans. Microw. Theory Techn, vol. 65, no. 3, pp. 923–933, 3. 2017. doi: 10.1109/TMTT.2016.2627554.

[112]. Ostadrahimi M, Zakaria A, LoVetri J, and Shafai L, “A near-field dual polarized (TE–TM) microwave imaging system,” IEEE Trans. Microw. Theory Techn, vol. 61, no. 3, pp. 1376–1384, 3. 2013. doi: 10.1109/TMTT.2012.2237181.

[113]. Yu C et al., “Active microwave imaging II: 3-D system prototype and image reconstruction from experimental data,” IEEE Trans. Microw. Theory Techn, vol. 56, no. 4, pp. 991–1000, 2008. doi: 10.1109/TMTT.2008.919661.

[114]. Henriksson T, Joachimowicz N, Conessa C, and Bolomey JC, “Quantitative microwave imaging for breast cancer detection using a planar 2.45 GHz system,” IEEE Trans. Instrum. Meas, vol. 59, no. 10, pp. 2691–2699, 2010. doi: 10.1109/TIM.2010.2045540.

[115]. Guardiola M, Capdevila S, Blanch S, Romeu J, and Jofre L, “UWB high-contrast robust tomographic imaging for medical applications,” in Proc. Int. Conf. Electromagnetics in Advance Applications, 2009, pp. 560–563. doi: 10.1109/ICEAA.2009.5297370.

[116]. Guardiola M, Capdevila S, and Jofre L, “UWB biFocusing tomography for breast tumor detection,” in Proc. 3rd Euro. Conf. Antennas and Propagation, 2009, pp. 1855–1859.

[117]. Guardiola M, Jofre L, Capdevila S, Blanch S, and Romeu J, “3d UWB magnitude-combined tomographic imaging for biomedical applications. Algorithm validation,” Radioengineering, vol. 20, no. 2, pp. 366–372, 2011.

[118]. Lazaro A, Girbau D, and Villarino R, “Simulated and experimental investigation of microwave imaging using UWB,” Prog. Electromagn. Res, vol. 94, pp. 263–280, 2009. doi: 10.2528/PIER09061004.

[119]. Lazaro A, Girbau D, and Villarino R, "Wavelet-Based breast tumor localization technique using a UWB radar," Prog. Electromagn. Res, vol. 98, pp. 75–95, 2009. doi: 10.2528/PIER09100705.

[120]. Zhang D and Mase A, "Experimental study on radar-based breast cancer detection using UWB antennas without background subtraction," Biomed. Eng. Appl. Basis Commun, vol. 23, no. 5, pp. 383–391, 2011. doi: 10.4015/S1016237211002712.

[121]. Lai JCY, Soh CB, Gunawan E, and Low KS, "UWB microwave imaging for breast cancer detection: Experiments with heterogeneous breast phantoms," Prog. Electromagn. Res. M, vol. 16, pp. 19–29, 2011. doi: 10.2528/PIERM10072001.

[122]. Amin MG and Ahmad F, "Wideband synthetic aperture beamforming for through-the-wall imaging," IEEE Signal Process. Mag, vol. 25, no. 4, pp. 110–113, 7 2008. doi: 10.1109/MSP.2008.923510.

[123]. Debes C, Amin MG, and Zoubir AM, "Target detection in single-and-multiple-view through-the-wall radar imaging," IEEE Trans. Geosci. Remote Sens, vol. 47, no. 5, pp. 1349–1361, 5 2009. doi: 10.1109/TGRS.2009.2013460.

[124]. Debes C, Zoubir AM, and Amin MG, "Enhanced detection using target polarization signatures in through-the-wall radar imaging," IEEE Trans. Geosci. Remote Sens, vol. 50, no. 5, pp. 1968–1979, 5 2012. doi: 10.1109/TGRS.2011.2170077.

[125]. Liu X, Leung H, and Lampropoulos GA, "Effect of wall parameters on ultra-wideband synthetic aperture through-the-wall radar imaging," IEEE Trans. Aerosp. Electron. Syst, vol. 48, no. 4, pp. 3435–3449, 10. 2012. doi: 10.1109/TAES.2012.6324724.

[126]. Li J, Zeng Z, Sun J, and Liu F, "Through-wall detection of human being's movement by UWB radar," IEEE Geosci. Remote Sens. Lett, vol. 9, no. 6, pp. 1079–1083, 11. 2012. doi: 10.1109/LGRS.2012.2190707.

[127]. Wu S, Tan K, Xia Z, Chen J, Meng S, and Guangyou F, "Improved human respiration detection method via ultra-wideband radar in through-wall or other similar conditions," IET Radar Sonar Navig, vol. 10, no. 3, pp. 468–476, 2. 2016. doi: 10.1049/ietrsn.2015.0159.

[128]. Liang X, Zhang H, Fang G, Ye S, and Gulliver TA, "An improved algorithm for through-wall target detection using ultra-wideband impulse radar," IEEE Access, vol. 5, pp. 22,101–22,118, 10. 2017. doi: 10.1109/ACCESS.2017.2761771.

[129]. Akduman I, Crocco L, and Soldovieri F, "Experimental validation of a simple system for through-the-wall inverse scattering," IEEE Geosci. Remote Sens. Lett, vol. 8, no. 2, pp. 258–262, 3. 2011. doi: 10.1109/LGRS.2010.2065212.

[130]. Wang F, Horng T, Peng K-C, Jau J-K, Li J-Y, and Chen C-C, "Detection of concealed individuals based on their vital signs by using a see-through-wall imaging system with a self-injection-locked radar," IEEE Trans. Microw. Theory Techn, vol. 61, no. 1, pp. 696–704, 1. 2013. doi: 10.1109/TMTT.2012.2228223.

[131]. Fioranelli F, Salous S, and Raimundo X, "Frequency-modulated interrupted continuous wave as wall removal technique in through-the-wall imaging," IEEE Trans. Geosci. Remote Sens, vol. 52, no. 10, pp. 6272–6283, 10. 2014. doi: 10.1109/TGRS.2013.2295835.

[132]. Dang V and Kilic O, "Simulation framework for compressive sensing-based through-wall detection of moving targets," IET Radar Sonar Navig, vol. 11, no. 9, pp. 1349–1358, 9. 2017. doi: 10.1049/iet-rsn.2017.0012.

[133]. Odedo VC, Yavuz ME, Costen F, Himeno R, and Yokota H, "Time reversal technique based on spatiotemporal windows for through the wall imaging," IEEE Trans. Antennas Propag, vol. 65, no. 6, pp. 3065–3072, 6 2017. doi: 10.1109/TAP.2017.2696421.

[134]. Soldovieri F, Solimene R, and Ahmad F, "Sparse tomographic inverse scattering approach for through-the-wall radar imaging," IEEE Trans. Instrum. Meas, vol. 61, no. 12, pp. 3340–3350, 12. 2012. doi: 10.1109/TIM.2012.2210454.

[135]. Sheen DM, McMakin DL, and Hall TE, "Three-dimensional millimeter-wave imaging for concealed weapon detection," IEEE Trans. Microw. Theory Techn, vol. 49, no. 9, pp. 1581–1592, 9. 2001. doi: 10.1109/22.942570.

[136]. Sheen D, McMakin D, and Hall T, "Near-field three-dimensional radar imaging techniques and applications," Appl. Opt, vol. 49, no. 19, pp. E83–E93, 2010. doi: 10.1364/AO.49.000E83. [PubMed: 20648125]

[137]. Zhuge X and Yarovoy AG, “A sparse aperture MIMO-SAR-based UWB imaging system for concealed weapon detection,” IEEE Trans. Geosci. Remote Sens, vol. 49, no. 1, pp. 509–518, 1. 2011. doi: 10.1109/TGRS.2010.2053038.

[138]. Zhuge X and Yarovoy A, “Automatic target recognition in ultra-wideband 3-D images for concealed weapon detection,” in Proc. 9th European Conf. Synthetic Aperture Radar, 4. 2012, pp. 186–188.

[139]. Agarwal S, Kumar B, and Singh D, “Non-invasive concealed weapon detection and identification using V band millimeter wave imaging radar system,” in Proc. Nat. Conf. Recent Advances Electronics and Computer Engineering (RAECE), 2. 2015, pp. 258–262. doi: 10.1109/RAECE.2015.7510202.

[140]. Jaisle KP and Rappaport CM, “Ray-based reconstruction algorithm for multi-monostatic radar in imaging systems,” in Proc. IEEE Int. Symp. Antennas and Propagation and USNC/URSI Nat. Radio Sci. Meeting, 7 2017, pp. 405–406. doi: 10.1109/APUSNCURSINRSM.2017.8072245.

[141]. Knipper R et al., “THz absorption in fabric and its impact on body scanning for security application,” IEEE Trans. THz Sci. Technol, vol. 5, no. 6, pp. 999–1004, 11. 2015. doi: 10.1109/TTHZ.2015.2474115.

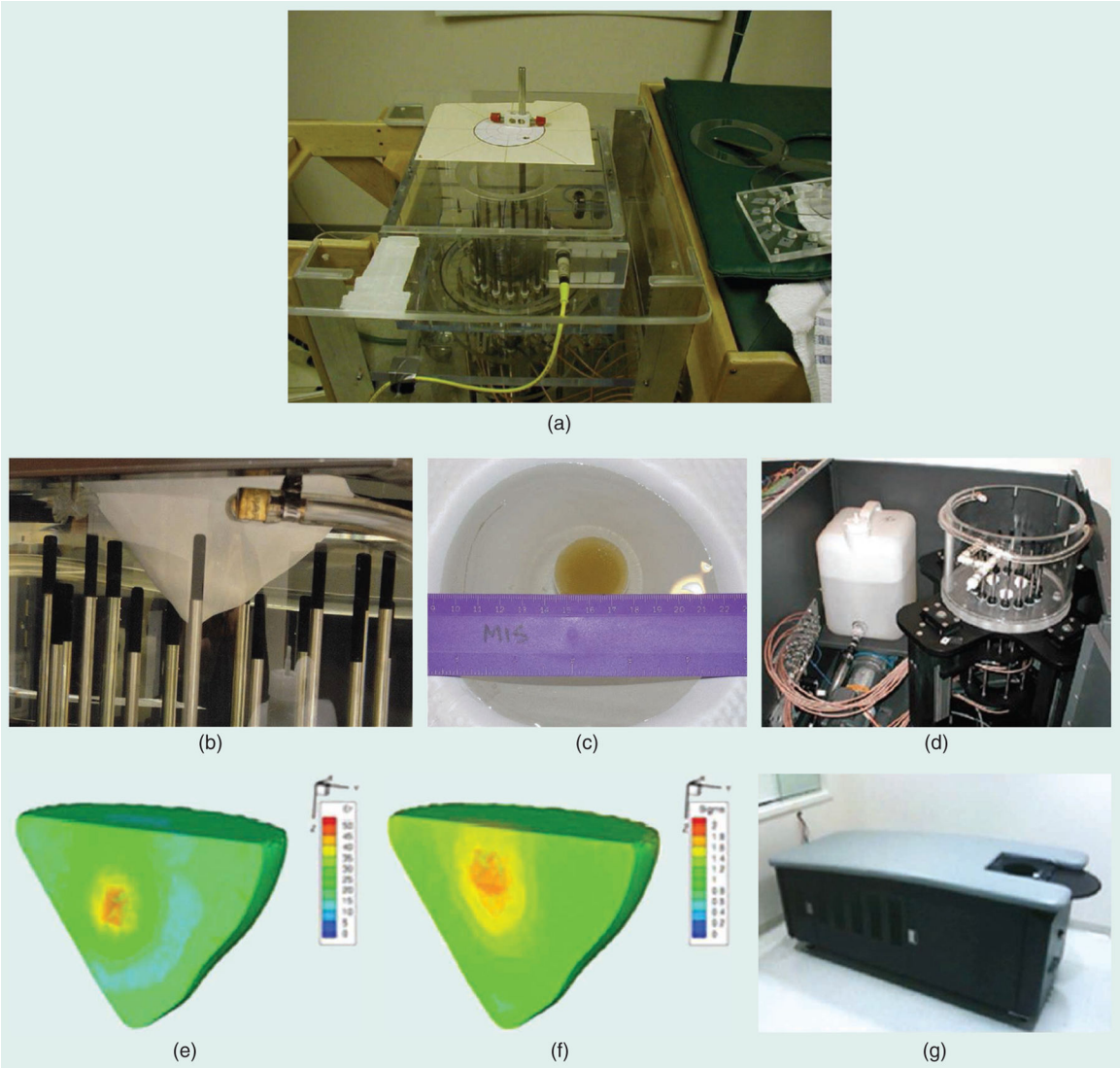

Figure 1.

(a) The microwave breast-imaging system set up at Dartmouth College. (Reproduced from [25]; used with permission of AUR.) Sixteen monopole antennas are immersed in a tank filled with a coupling liquid. (b) The side view of the breast phantom. (c) The top view of the breast phantom and target inclusion [26]. (d) The illumination chamber and coupling-medium reservoir of the 3G system. The (e) reconstructed permittivity and (f) conductivity at 1,500 MHz, incorporating three XP transmissions of data in the reconstruction. (g) The 3G breast-imaging system. (Reproduced from [27]; used with permission of AIP Publishing.)

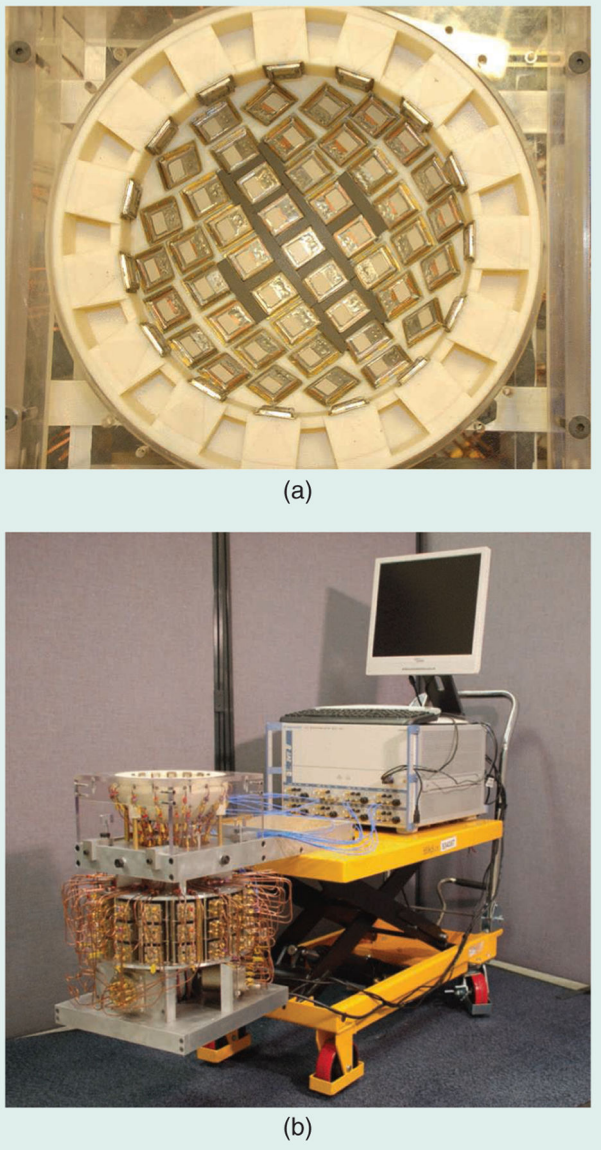

Figure 2.
The UWB breast-cancer imaging system developed at the University of Bristol [33]. (a) The UWB conformal antenna array consisting of 60 slot-antenna elements. (b) The switching network (bottom) connects the UWB antenna array (top) and the eight-port VNA.

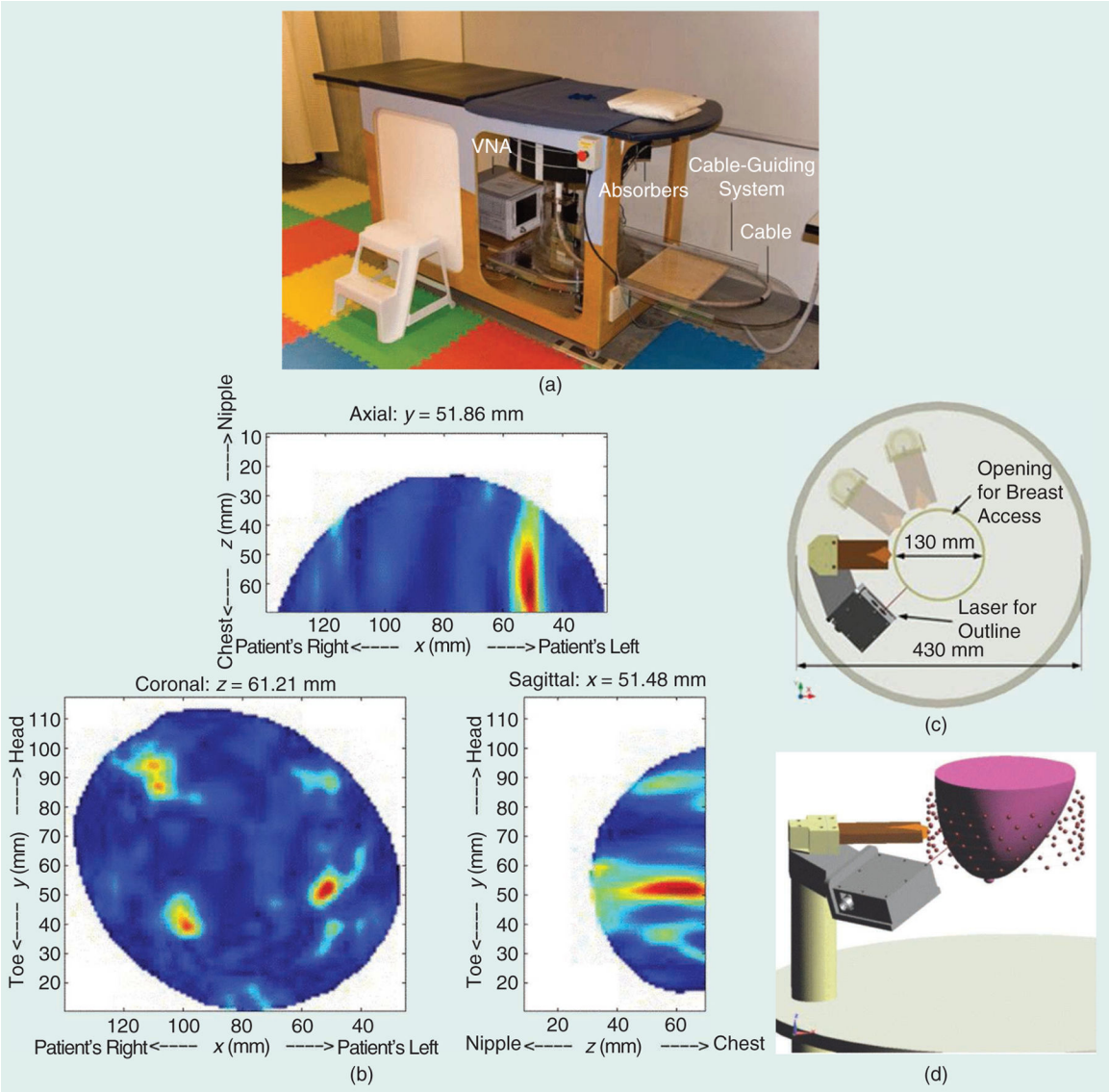

Figure 3.

The monostatic, radar-based microwave breast-imaging system prototype developed at the University of Calgary [38]. (a) The prototype system. (b) Patient images that were reconstructed using a confocal-imaging algorithm [39] on data collected by the system. The (c) top- and (d) side-view schematics of the antenna and laser that can move around the breast.

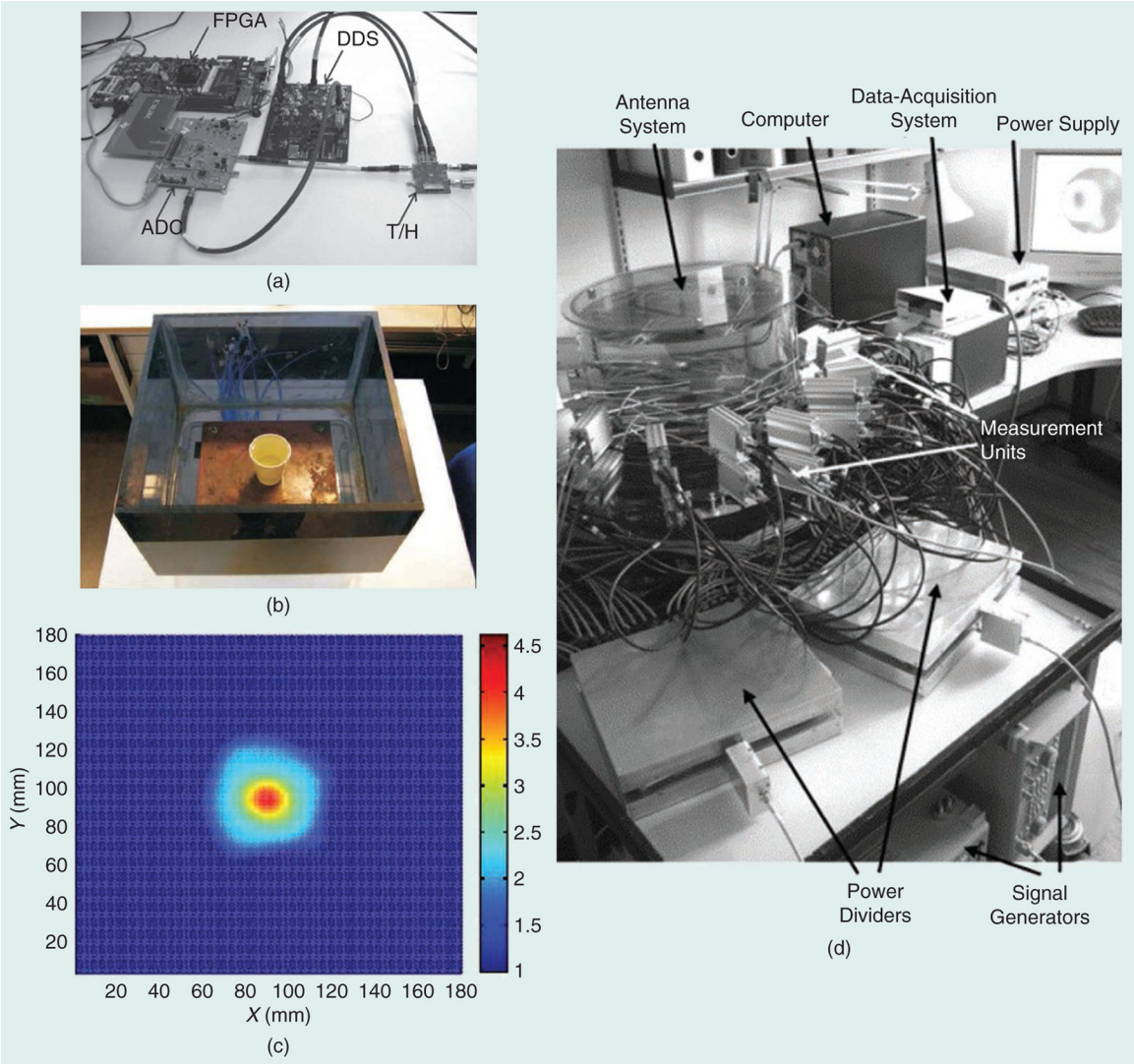

Figure 4.

The time-domain microwave system for medical diagnostics at CUT [44]. (a) The receiver system by Persson's research group. (b) A plastic cup of vegetable oil is placed at the center of the monopole antenna array. (c) A reconstructed image of the cup of vegetable oil. (d) The system developed by Rubaek's research group [45].

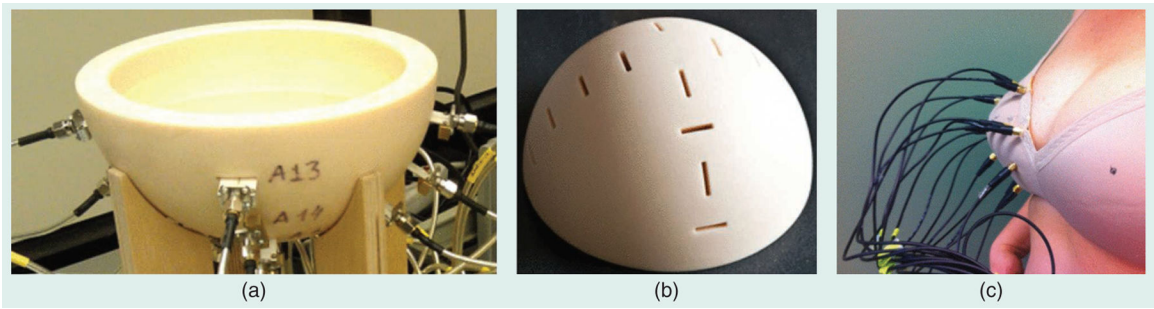

Figure 5.

The time-domain measurement system for breast imaging developed at McGill University. The (a) radome to house the antennas for (b) a table-based prototype [47]-[51]. (c) The bra-based measurement system [52].

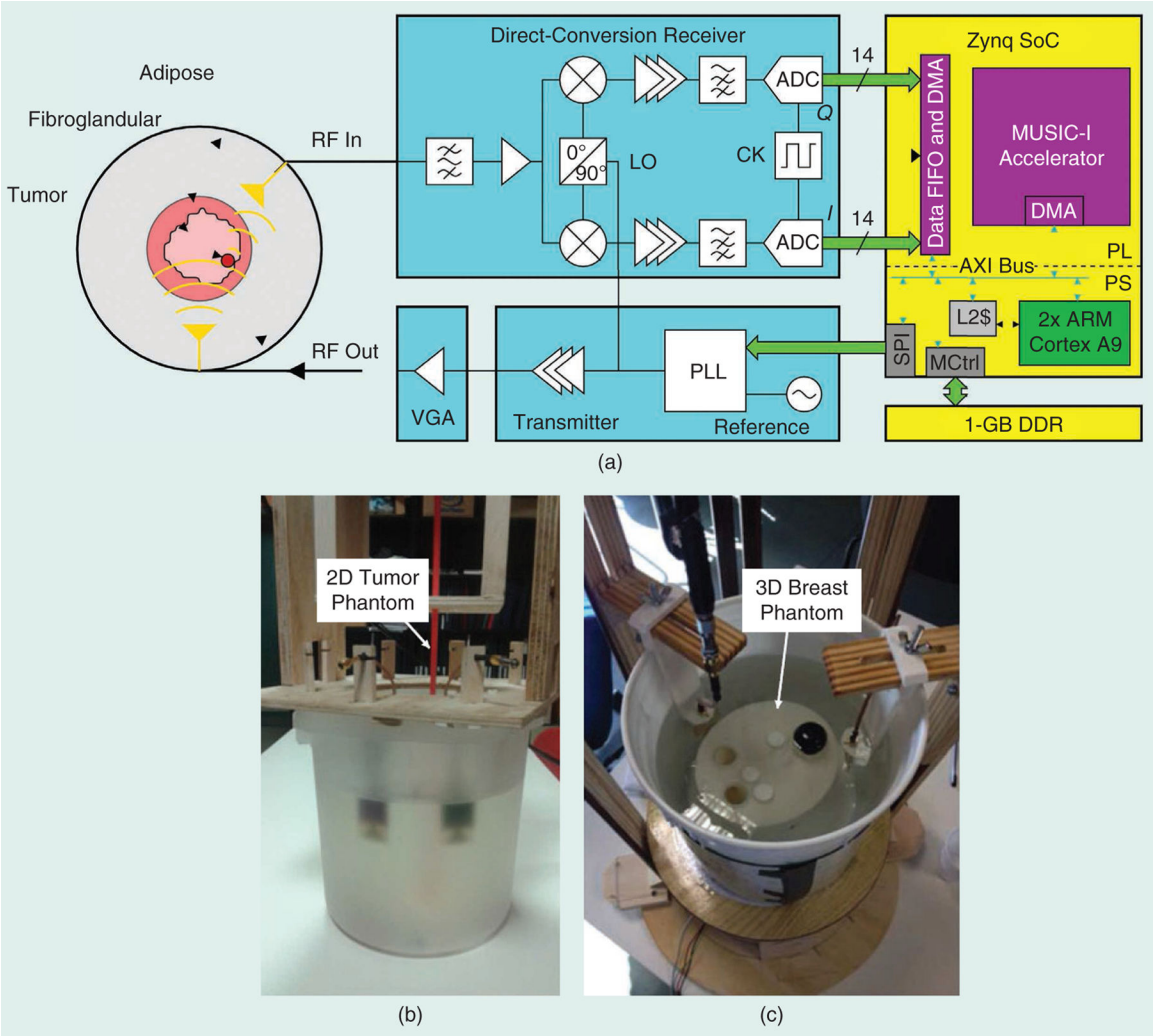

Figure 6.

The microwave-imaging breast-cancer detection system developed at Politecnico di Torino [56]. (a) The architecture of the prototype system. The (b) 2D and (c) 3D trial setups. VGA: video-graphics adapter; PLL: phase-locked loop; SoC: system on chip; FIFO: first in, first out; DMA: direct memory access; AXI: advanced extensible interface; SPI: serial peripheral interface; CK: clock; PL: programmable logic; PS: processing system; Q: quadrature; I: in-phase.

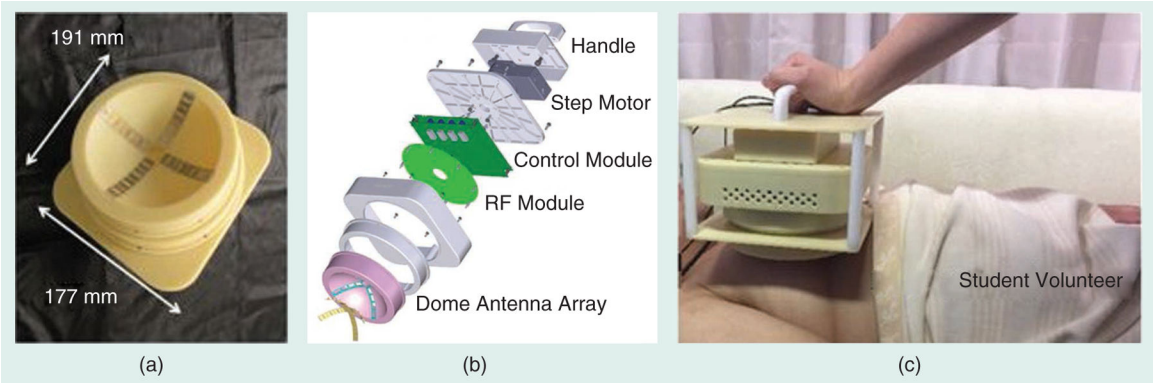

Figure 7.

The hand-held breast-tumor detector developed by Kikkawa's group [57]. (a) The probe, which is a dome antenna array. (b) A diagram of the system. (c) The system being used on a volunteer.

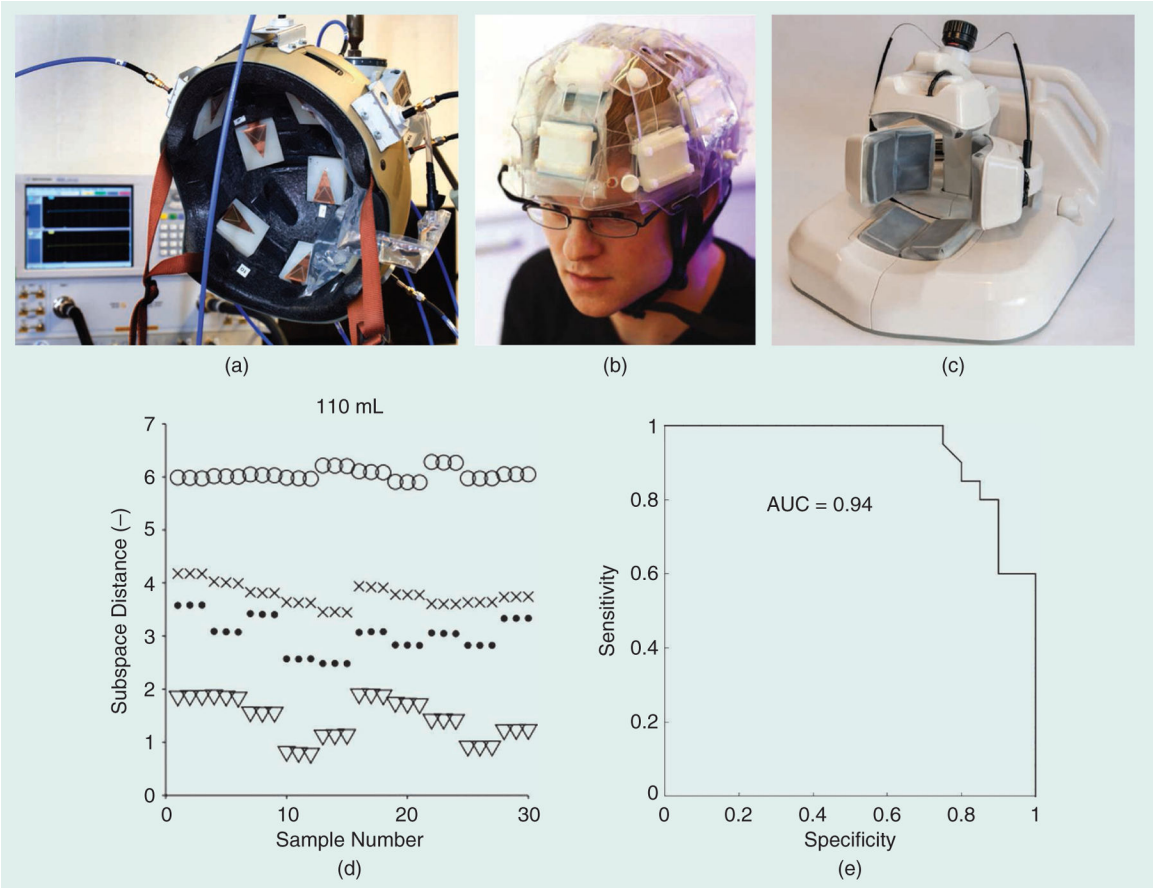

Figure 8.

The antenna array developed for brain-stroke detection at CUT [69]. (a) Ten patch antennas are mounted on a helmet, with plastic bags holding the matching liquid. (b) Twelve patch antennas are mounted on a custom-built supporting structure. (c) Eight antennas are mounted in an array that can be adjusted to fit the patient [14]. (d) The distances, d_c, to each subspace for all observations using the 110-mL, intracranial-bleeding head phantoms. (Reproduced from [70]; used with permission of Springer Nature Switzerland AG.) (e) The ROC curve to distinguish subdural hematoma patients from healthy subjects. (Reproduced from [71]; used with permission of Mary Ann Liebert, Inc.)

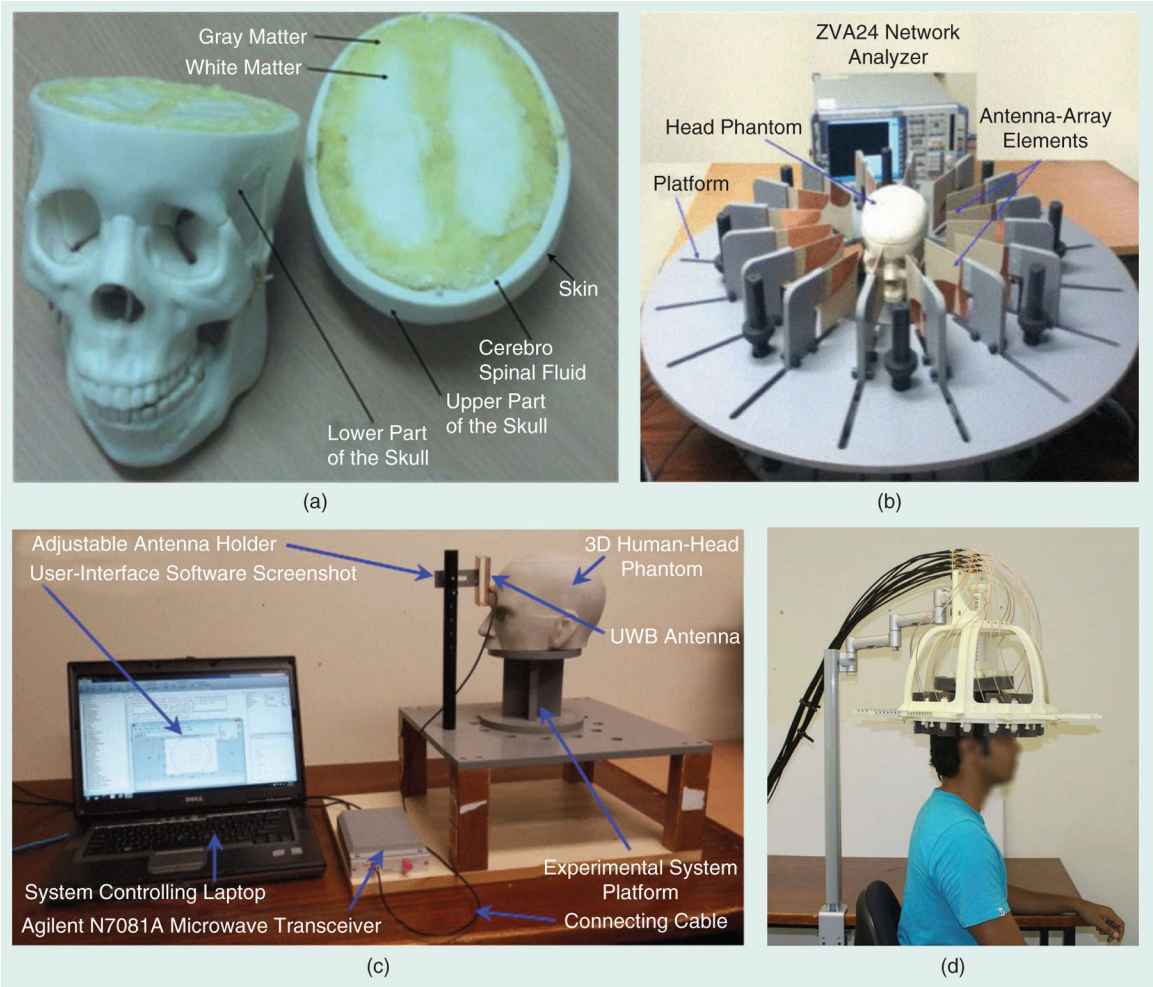

Figure 9.

The head-phantom and monostatic imaging system for brain-stroke detection developed at the University of Queensland. (a) The head phantom. (b) The antenna array consisting of 16 corrugated tapered-slot antennas on a rotatable platform [72], [74]. (c) The second system, composed of one fixed antenna, and the phantom on a rotatable support [75]. (d) The third system, with 16 fixed antennas. (Source: [77].)

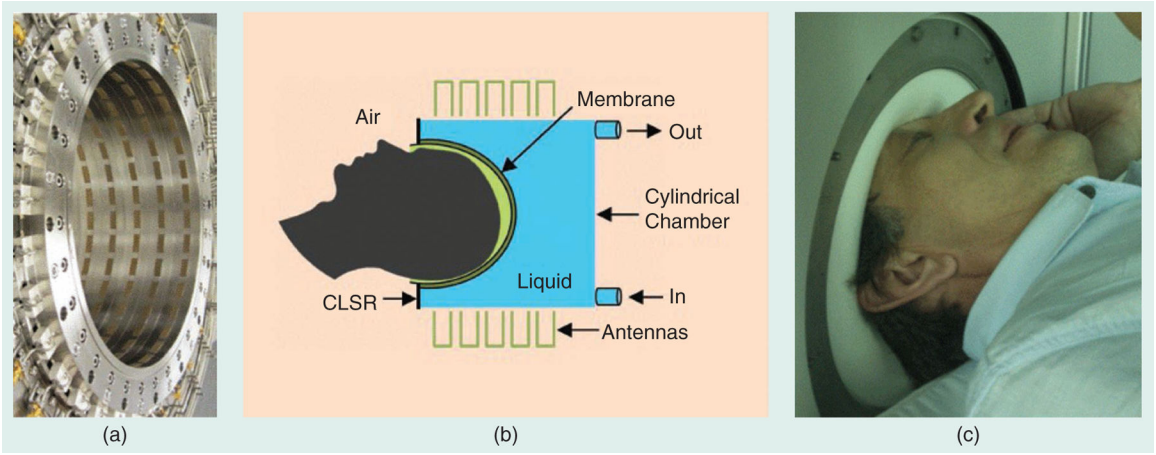

Figure 10.

The brain-stroke imaging prototype system developed by EMTensor [78], [79]. (a) The chamber with 160 antennas in five rings. (b) The architecture of the chamber. (c) A human-head measurement made with the prototype system. CLSR: carbon-loaded silicone rubber.

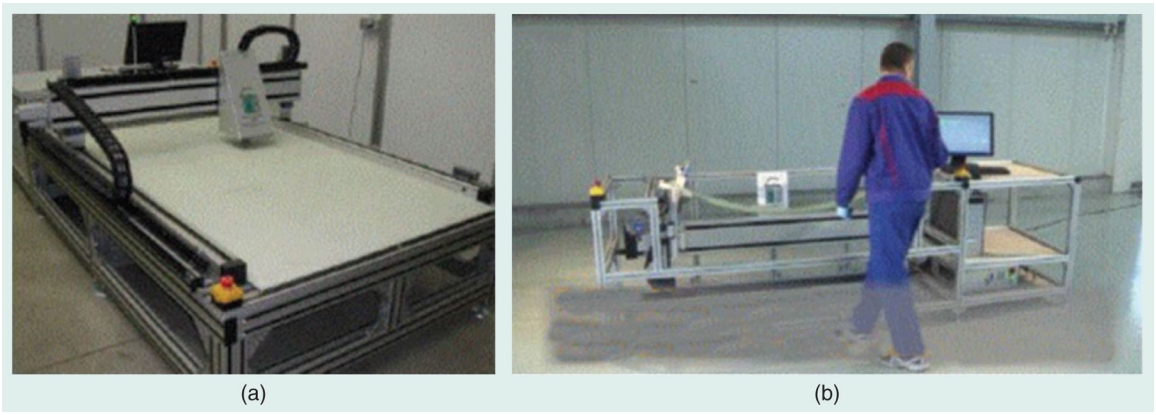

Figure 11.
Stationary microwave test systems [95] for (a) planar substrates and (b) glass-fiber reinforced-plastic leaf springs for automobiles. (Source: [95]; used with permission.)

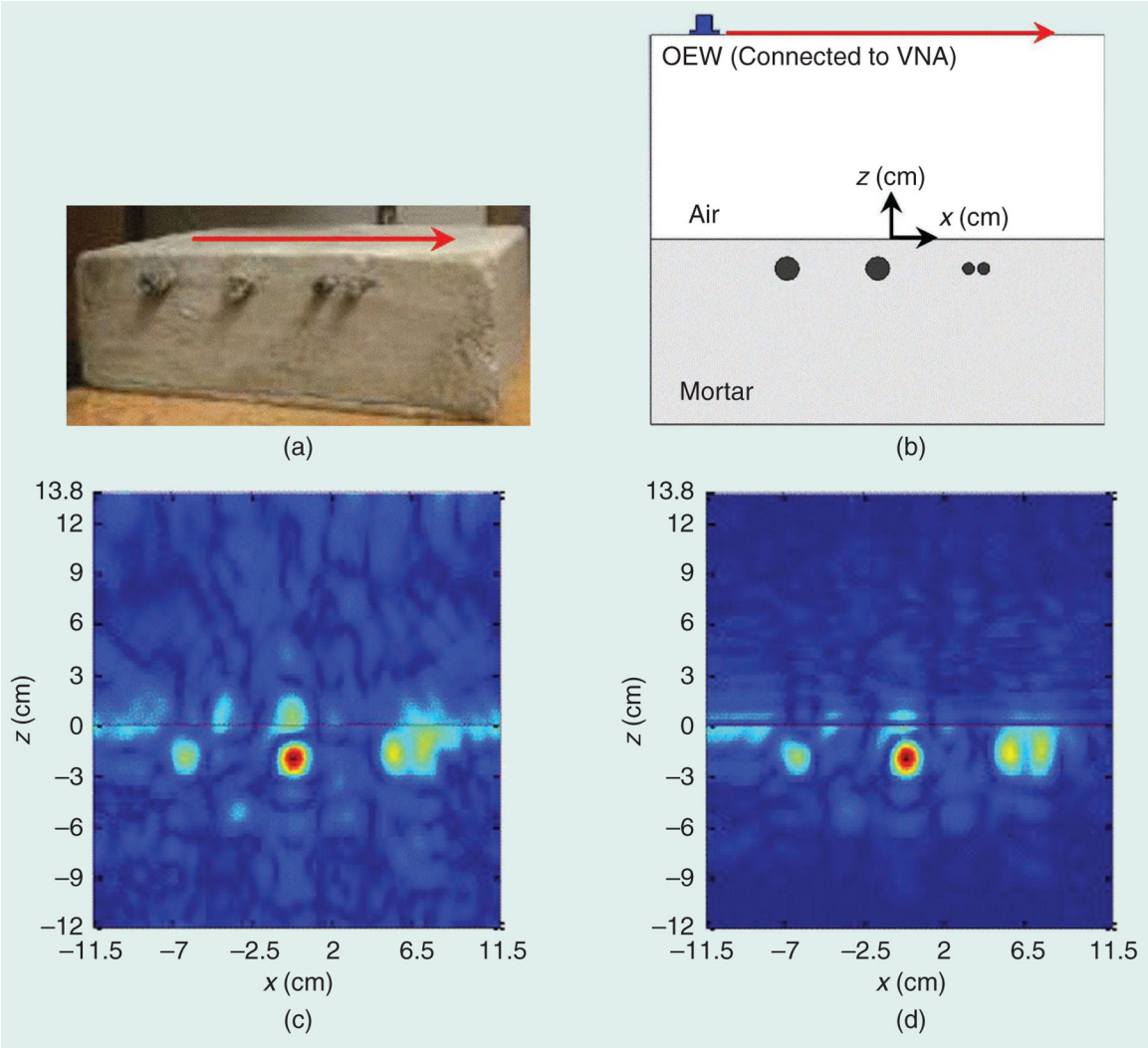

Figure 12.

The microwave ND-detection experiment conducted at the Missouri University of Science and Technology [96]. (a) A mortar specimen with four rebars under test. (b) The schematic diagram of the experiment setup: a probe connected to a VNA moves along the surface of the mortar specimen to collect reflection coefficients. (c) The reconstructed image from a piecewise SAR algorithm. (d) The reconstructed image from a Wiener-filter–based layered SAR algorithm. OEW: open-ended rectangular waveguide.

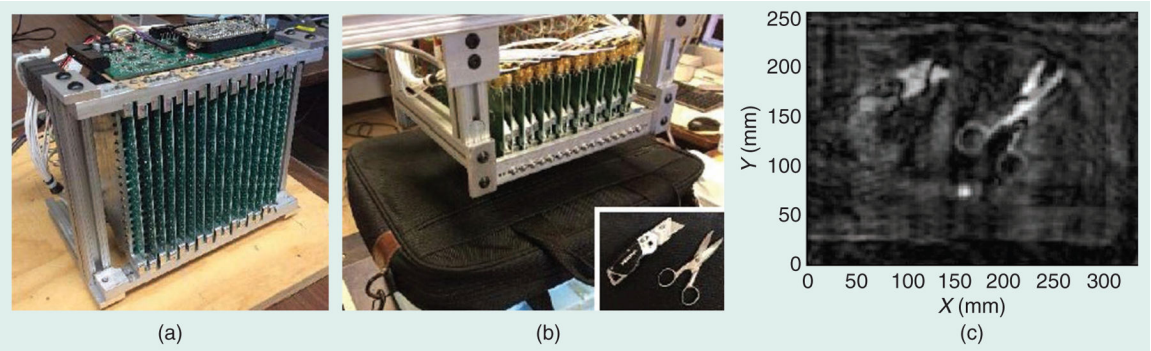

Figure 13.

The WB microwave camera by Zhougi's group [97]. (a) The front side of the 1D antenna array, showing the array aperture. (b) The laptop bag in front of the camera aperture, with an inset displaying the objects inside the bag: a box cutter and scissors. (c) The 2D image slice focused on the scissors.

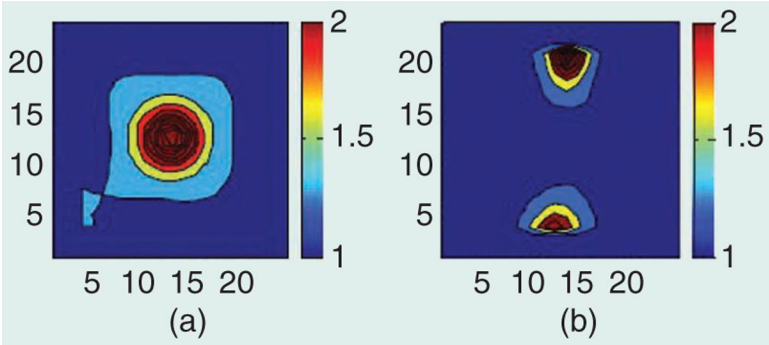

Figure 14.

The Wu group's reconstructed images of flow pipes at 4 GHz. (a) The image reconstruction at the last iteration for the first dielectric phantom. (b) The image reconstruction at the last iteration for the second dielectric phantom. (Source: [98]; used with permission.)

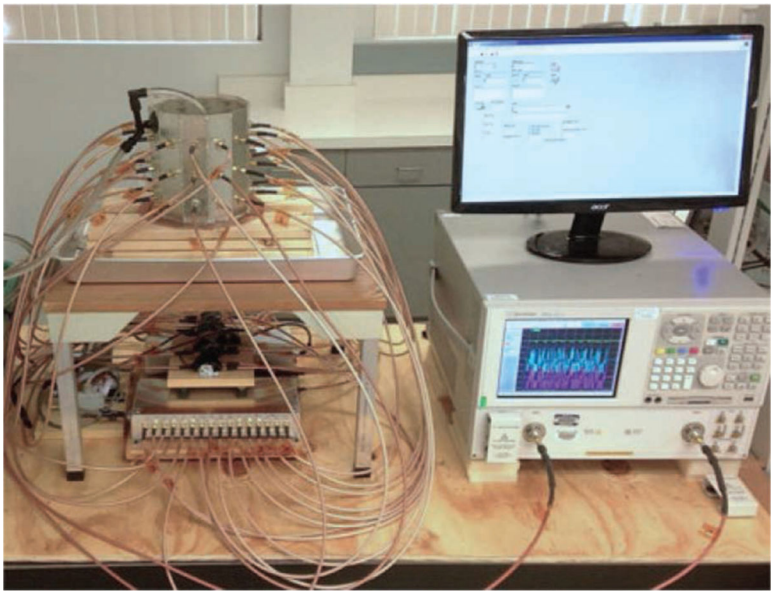

Figure 15.
The microwave-imaging differential-temperature-monitoring measurement system developed at the University of Southern California [101].

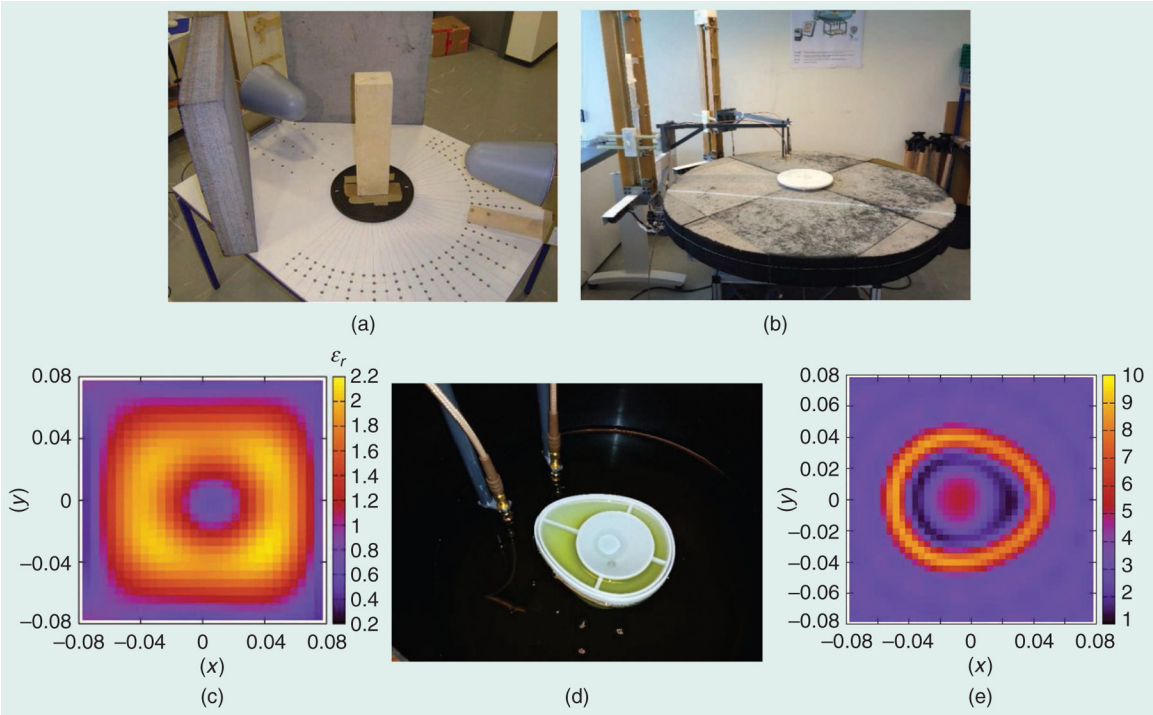

Figure 16.

The microwave measurement system by collaborators from the University of Applied Sciences of Southern Switzerland, Centro di Senologia della Svizzera, and the University of Genoa [102], [104]. (a) The setup for the frequency-domain measurement of a wood slab. (b) The setup for the frequency-domain measurement a breast phantom, including the plastic extension-arms system. (c) The reconstructed image of the wood slab. (d) The breast phantom. (e) The image of the breast-phantom object that was reconstructed using the inversion algorithm in [105].

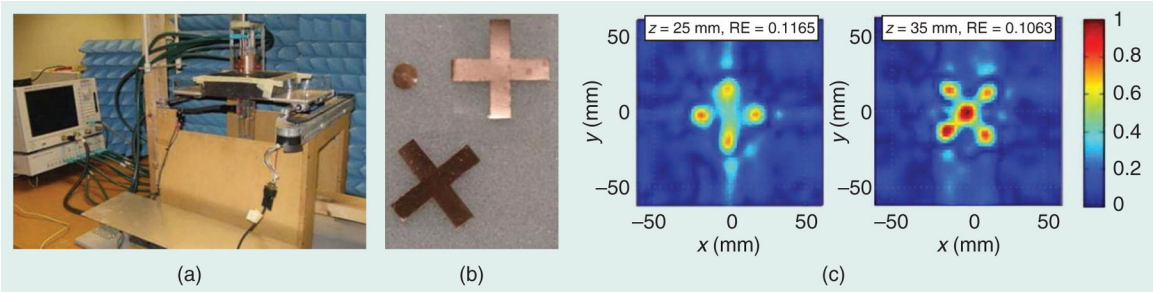

Figure 17.

The microwave-measurement system developed at McMaster University [18]. (a) The setup for the frequency-domain measurement. (b) The X-shaped metallic targets. (c) The reconstructed images of the X-shaped metallic targets when placed at two different locations.

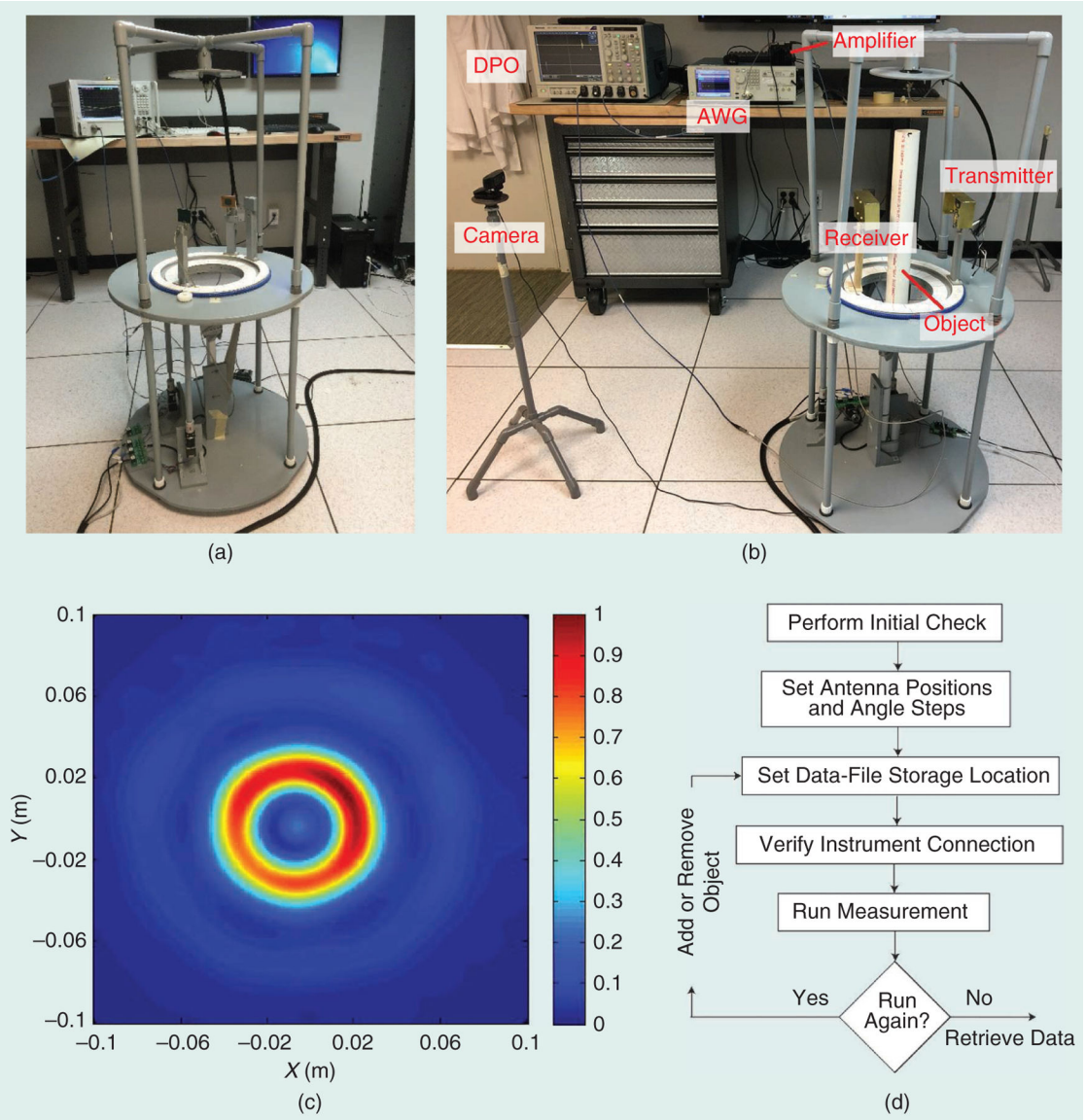

Figure 18.

The microwave-measurement system by Ellumen, which has a controllable antenna movement in a transmit–receive mode. The setups for the (a) frequency-domain [107] and (b) time-domain measurement [108]. (c) An image of the cylindrical object that was reconstructed with a phase confocal-imaging algorithm [110] using data collected by the system in [107]–[109]. (d) A diagram of the software's important operation steps. DPO: digital phosphor oscilloscope; AWG: arbitrary waveform generator.

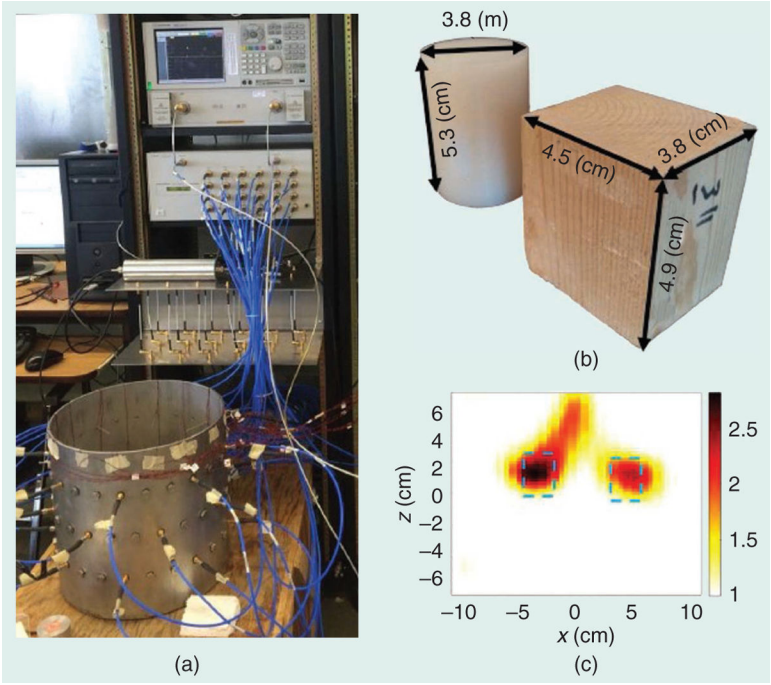

Figure 19.

The microwave-measurement system developed at the University of Manitoba [111]. (a) The setup for the frequency-domain measurement. (b) The wood cube and nylon cylinder. (c) The reconstructed image of the wood cube and nylon cylinder at 1.75 GHz.

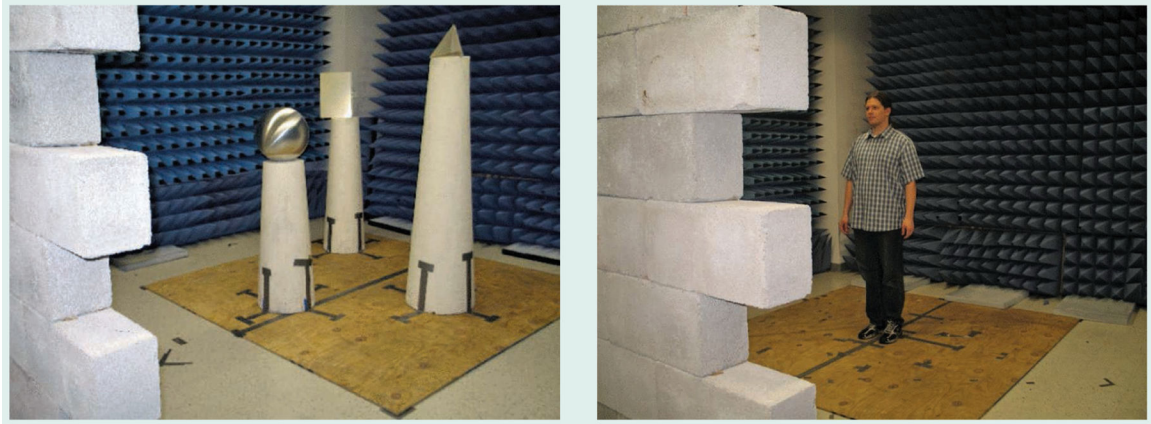

Figure 20.
Tests for through-the-wall radar imaging produced by a collaboration between AGT Group, Technische Universität Darmstadt, and Villanova University [124]. (a) Differently shaped objects located behind a wall. (b) A man behind the wall.

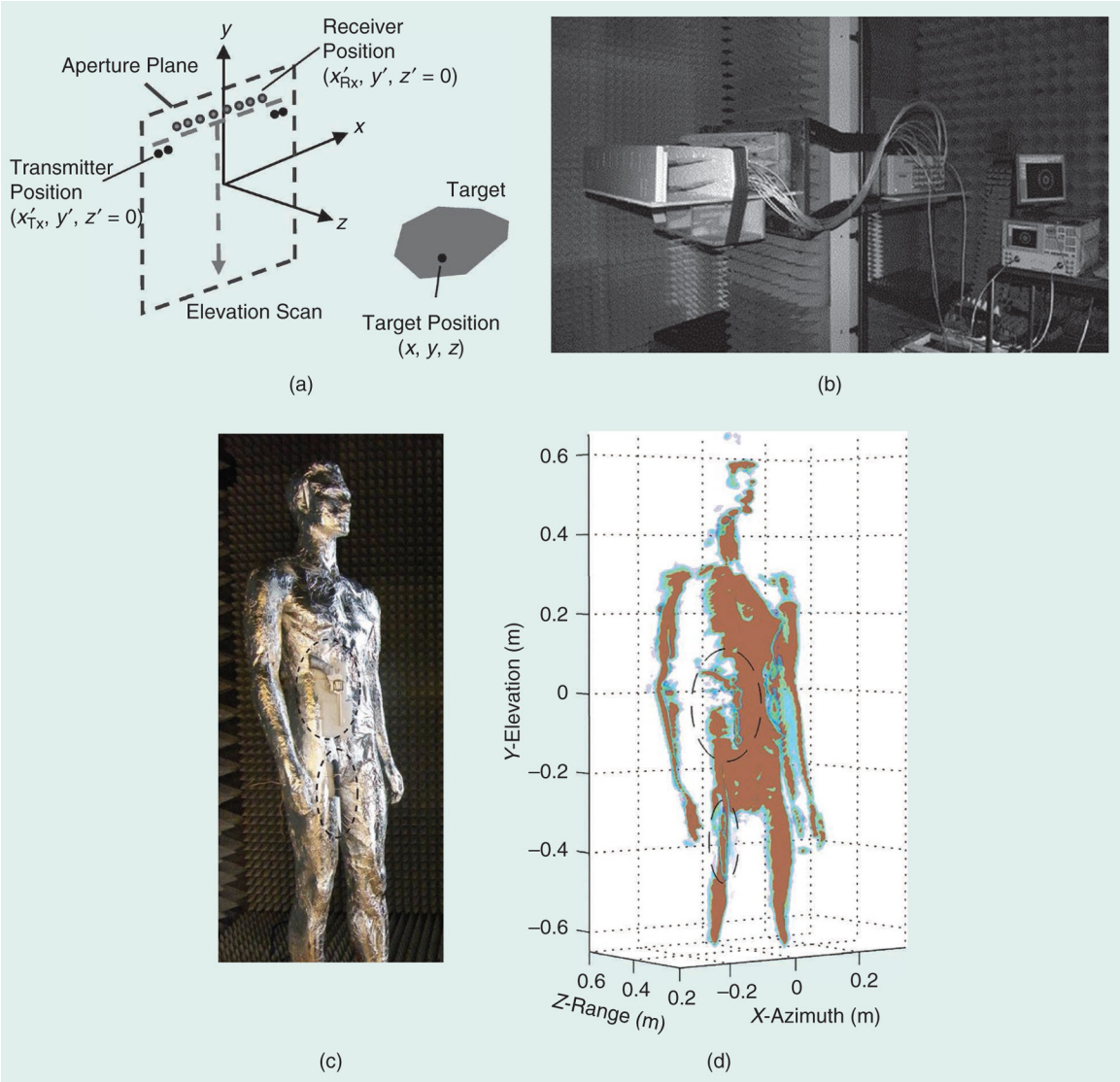

Figure 21.

The UWB MIMO-SAR measurement-system setup with a network analyzer in an anechoic chamber at the Delft University of Technology, The Netherlands [137]. (a) A schematic diagram of the MIMO-array structure and its movement for a scan. (b) The MIMO-SAR configuration with an additional multiport switch. (c) A gun and knife attached to a mannequin covered with aluminum foil and (d) the 3D-imaging result.

TABLE 1.

Microwave breast-imaging detection systems.

Group	Antennas	Frequency	Hardware	Coupling Liquid
Meaney [27]	Multistatic, 16 monopoles	500 MHz–3 GHz	AD/LO	Yes
Hagness [29]	Monostatic, one UWB transceiver antenna	1–11 GHz	VNA	Yes
Craddock [35]	Multistatic, 60 elements	3–8 GHz	VNA	Yes
Fear [40]	Monostatic, one UWB transceiver antenna	2.4–12 GHz	VNA	Yes
Persson [44]	Multistatic, 20 monopoles	800 MHz–3.8 GHz	ADC/FPGA	No
Rubaek [45]	Multistatic, 32 monopoles	0.3–3 GHz	RF analog signal generator/ADC	Yes
Popovic [52]	Multistatic, 16 monopoles	2–4 GHz	Picoscope	No
Vipianna [56]	Multistatic, two WB monopoles	1.4–1.6 GHz	FPGA	Yes
Kikkawa [57]	Multistatic, 16 elements, planar-slot UWB	3.1–10.6 GHz	ADC/CMOS	No
Jeon [59]	Multistatic, 16 monopoles	500 MHz–3 GHz	AD/signal source	Yes
Chen [61]	Multistatic, two horn antennas	4–8.5 GHz	VNA	Yes
Kuwahara [63]	Multistatic, six, 18, or 30 elements	4–9 GHz	VNA	No

TABLE 2.

Microwave brain-imaging detection systems.

Group	Antennas	Frequency	Hardware	Coupling Liquid
Persson [71]	Multistatic, eight antennas	0.1–1.95 GHz	VNA	No
Abbosh [75]	Monostatic, 16 antenna elements	1–2.4 GHz	VNA	No
EMTensor [79]	Multistatic, 160 antennas	0.9–1.8 GHz	VNA	Yes

TABLE 3.

Selected NDT detection systems.

Group	Antennas	Frequency	Hardware	Coupling Liquid
Zoughi [97]	Monostatic, 256 elements	20–30 GHz	VCO/ADC	No
Wu [98]	Multistatic, 16 elements	2–4 GHz	VNA	No
Moghaddam [101]	Multistatic, 32 elements	915 MHz	VNA	Yes
Pastorino [104]	Multistatic, two elements	2–10 GHz	VNA	Yes
Nikolva [18]	Multistatic, two elements	3.1–10.6 GHz	VNA	No
Ellumen [108]	Multistatic, two elements	2–7 GHz	VNA or oscilloscope	No
LoVetri [111]	Multistatic, 12 elements	3–5 GHz	VNA	No
Liu [113]	Multistatic, two elements	1.74 GHz	VNA	Yes
Bolomey [114]	Multistatic, two elements	2.45 GHz	VNA	Yes
Jofre [117]	Multistatic, two elements	3–10 GHz	VNA	No
Villarino [119]	Multistatic, two elements	3.1–10.6 GHz	Pulse generator/sampler converter	Yes
Mase [120]	Multistatic, two elements	1–10 GHz	Oscilloscope	Yes
Low [121]	Multistatic, two elements	2.4–12 GHz	Oscilloscope	No